AN ABSTRACT OF THE THESIS OF

Huei-I Huang for the degree of Master of Science in Atmospheric Sciences presented on 24 May, 1988.

Title: The Long-Term Variations of East Asia Jet Stream In The Wintertime

Abstract approved: Redacted for Privacy

Using rotated principal component analysis, 200mb wind data from the First GARP Global Experiment are analyzed in the East Asia winter monsoon region. It is found that there exist slowly eastward-moving disturbances with a wind-speed maximum embedded in the jet stream (jet streak). The implied vertical circulation that is transverse to the jet streak is thermally direct in the entrance region of jet streak and thermally indirect in the exit region.

The Lagrangian momentum equation for transient part of the flow indicates that the magnitude of westerly acceleration of an air parcel moving through the jet streak is related to the Coriolis acceleration of the transient ageostrophic flow, the advection of mean momentum by transient flow and momentum conversion between mean and transient flow due to transient eddies. Estimates of terms in this equation in the entrance region of jet streak suggest that the increase of westerly momentum due to the Coriolis acceleration of the

ageostrophic flow is mostly balanced by the decrease due to the mean easterly momentum advection by the transient jet-streak flow. Thus, the confluence theory of Namias and Clapp (1949) appears to be valid for the slowly moving jet streaks in the East Asia jet stream.

THE LONG-TERM VARIATIONS OF EAST ASIA JET STREAM IN THE WINTERTIME

by

Huei-I Huang

A THESIS

submitted to

Oregon State University

in partial fulfillment of
the requirements for the
degree of

Master of Science

Completed May 24, 1988
Commencement June, 1989

APPROVED:

Redacted for Privacy

Professor of Atmospheric Sciences in charge of major

Redacted for Privacy

Chairman of the Department of Atmospheric Sciences

Redacted for Privacy

Dean of Graduate School

Date thesis is presented: May 24, 1988

ACKNOWLEDGMENTS

I thank my advisor, Dr. Steve Esbensen, for his generous support and guidance without which I would not have been able to finish this study. I also thank Dr. Hua-Lu Pan for his invaluable advice concerning the rotated principal component model.

This material is based upon work supported by the National Science Foundation under Grant Nos. ATM-8718475 and ATM-8419548. The Government has certain rights in this material.

TABLE OF CONTENTS

LIST OF FIGURES

THE LONG-TERM VARIATIONS OF EAST ASIA JET STREAM IN THE WINTERTIME

CHAPTER 1: INTRODUCTION

During the northern winter, East Asia is dominated by the quasi-stationary Siberian high which is associated with strong subsidence, while over the equatorial maritime continents of Indonesia and Malaysia and the South China sea there is strong diabatic heating and upward mass flux due to deep cumulus convection. The large thermal contrast between the heat source over tropical region and the heat sinks over northern China and Siberia leads to a thermally direct monsoonal circulation in the wintertime. This circulation is usually referred to as the local Hadley circulation in which available potential energy is converted into kinetic energy to maintain the winter monsoonal circulation (Blackburn, 1985).

Another remarkable feature in the northern hemisphere winter is the subtropical jet stream over East Asia. According to the confluence theory of Namias and Clapp (1949) and the diagnostic study of Murakami (1981), the acceleration over the entrance

region of the time-mean stationary subtropical jet stream is maintained by the steady-state ageostrophic meridional flow at the jet stream level while the transient eddies are relatively unimportant. An observational study by Blackmon et al. (1977) gave additional evidence that a thermally direct circulation is required to provide the strong westerly acceleration over the jet entrance region where the transient eddy fluxes are found to be small, and to maintain the thermal wind equilibrium in the entrance region where the large-scale confluence induced by the Tibetan Plateau tends to increase the meridional temperature gradient.

Blackburn (1985) maintains that the acceleration over the jet entrance region is at least partially related to the rotational flow in the sense that the rotational component of wind is found to dominate the local energetics at the jet stream level; the divergent flow has a smaller contribution. Also, the vertical circulations associated with the acceleration of jet stream are confined near the jet axis with ascent at 20-30^{o}N, well away from the tropical convection zone. Thus, the diabatically forced component of the observed circulations plays a secondary role. This is in agreement with the results obtained by Pan and Zhou (1985). They suggested that the observed structure of the vertical circulation over East Asia winter monsoon region is the superposition of the local Hadley circulation and the secondary circulation associated with the East Asia jet stream. The upper

branch of the Hadley circulation has a strong southerly wind component in the upper tropical troposphere that decreases to zero at about 30°N. The secondary circulation has divergence (rising motion) south of the jet stream axis (20-30°N), maximum southerlies near the jet axis, and convergence (sinking motion) to the north of the jet stream (30-40°N).

Occasionally during the northern winter, the very cold air in the Siberian area suddenly moves equatorwards in the form of strong ageostrophic surface northeasterlies. This phenomenon is known as a cold surge which is characterized by an extensive freshening of low-level northeasterlies southwards to the South China sea. The surge is accompanied by northward sensible heat flux by the large-scale transient eddies and may be related to the intensity of tropical convection and the East Asia jet stream. Lau, Chang and Chan (1983) have proposed that the onset of cold surge is triggered by mid-latitude baroclinic disturbances.

Normally before the onset of the cold surge, an upper-level trough is situated to the south of the Tibetan Plateau and the associated vertical circulation over East Asia leads to a more intense Siberian high and weaker tropical convection; the jet stream tends to intensify to the north and weaken to the south. After the cold surge, a ridge is found over central China, the Siberian high is suppressed and the equatorial convection intensifies. The jet stream shifts southwards. These long-term

variations, according to Blackmon et al. (1977), involve primarily barotropic processes; baroclinicity seems to play little role.

There have been a number of studies of the midlatitude-tropical interactions associated with cold surge events. Chang and Lau (1980) present evidence suggesting that short-term midlatitude-tropical interactions occur when strong cold air advection strengthens the East Asia local Hadley circulation through increased sinking motion over northern China, which then intensifies the jet stream as a result of an increase of the upper-level meridional ageostrophic flow associated with the local Hadley circulation. The local Hadley circulation is also reinforced after the onset of a cold surge by increased convection in the equatorial region. Lau, Chang and Chan (1983) suggest that the fluctuations of the jet stream intensity reflect changes in eddy activity over the North Pacific as well as the intensity of the East Asia local Hadley circulation and the tropical convection. Nevertheless, using power spectrum analysis, Murakami (1981) found that the variance of the wintertime wind field is dominated by the long-term (10–30 day) variations; short-term (3–5 day) disturbances have much less power spectral density. Other studies (Lau and Lau, 1984; Pan and Zhou, 1985; Pan, 1987) have demonstrated the importance of the upper-level slowly eastward-propagating disturbances with about wavenumber 6, which are found to be similar to a midlatitude synoptic wave having divergence (rising motion) between the trough and the downstream

ridge, and convergence (sinking motion) between the trough and the upstream ridge. Pan and Zhou (1985) concluded that the midlatitude-tropical interactions over the East Asia winter monsoon region on the 10-20 day time scale are primarily the interactions between the eastward-moving long-synoptic-scale disturbances in the upper troposphere and the local winter monsoon circulation.

If the idea of Pan and Zhou (1985) and Blackburn (1985) that there exists two distinct vertical circulations in the East Asia winter monsoon area--one associated with the local Hadley circulation, the other with the jet stream--is true, it may be possible to separate these features by examining the variability of the system. The main objective of this study is to give a clear description of transient disturbances of the quasi-stationary jet stream. We will see that these disturbances take the form of slowly propagating jet streaks. We will examine the rotational and divergent winds associated with the jet streak, and the horizontal scale of the implied secondary circulations. The mechanisms maintaining the transient jet-streak flow will be discussed in a Lagrangian framework using the governing momentum equation. The primary diagnostic tool will be rotated principal component analysis (RPCA).

CHAPTER 2: DATA

Twice daily 200mb wind data over the East Asia winter monsoon region were selected from the FGGE IIIb data set prepared by ECMWF (see Bjorheim et al., 1981 for details). The data is archived on an 1.875x1.875^{o} latitude-longitude grid and covers the period December 1978 to February 1979. The divergent and rotational winds at 200mb are obtained using the standard spherical harmonics expansion method (Bourke et al.,1977). The data is low-pass filtered using a four-pole Butterworth filter (Shank, 1967; Guillemin, 1957) with a cut-off period of 10 days. It should be noted that the filter distorts approximately five-days' worth of data at the two ends of a time series.

Over the jet stream region, the magnitude of largest seasonal mean 200mb divergent component of zonal wind (u_{χ}) is only 3ms^{-1}, negligible in comparison with that of the rotational component whose magnitude is about 60ms^{-1}(Pan and Zhou, 1985). Therefore, the jet stream strength may be measured by the rotational component of the westerly wind. The divergent wind of the seasonal-mean flow in the region of 0-40^{o}N, 100-130^{o}E is primarily southerly (Pan and Zhou, 1985) so the local Hadley circulation may be represented by the divergent component of the meridional wind. The wind data of area 0-52.5^{o}N, 97.5-150^{o}E which includes the

jet entrance region and the East Asia winter monsoon circulation are submitted to rotated principal component analysis.

CHAPTER 3: DESCRIPTION OF METHODS

Rotated principal component analysis is a useful technique to reduce the dimensionality of a large set of data, such as the twice-daily wintertime wind data used in this study. This analysis has been widely used to examine the teleconnection patterns of the atmosphere (e.g. Horel, 1981). Since the basis of the rotated principal component analysis is empirical orthogonal function analysis (EOFA), the introduction will begin with EOFA.

3.1 Empirical Orthogonal Function Analysis

Empirical orthogonal function analysis transforms the original time series of spatial data into a set of orthogonal functions. The transformation begins with the following equation:

$$Z = F\ A^T \qquad (3.1)$$

where

Z= the Nxn matrix of the deviation of the wind from the time mean for each variable at each space gridpoint; N indexes number of observations and n is a combined index of variables and gridpoints

F= the new Nxn transformed variable matrix

A= an nxn transformation matrix

The original data matrix Z is transformed by Eq.(3.1) into a set of new variables (matrix F) which is obtained under the

following constraints: (a) new variables are uncorrelated with each other, i.e. orthogonal with respect to space; and (b) they are hierarchically ordered in terms of their variances with i-th new variable having i-th largest variance. Note that it is important to center the data set with respect to the mean value of each variable; in other words, the time mean must be removed prior to the decomposition (Preisendorfer, Zwiers and Barnett, 1981). If no centering were done, the coordinate-free feature of the principal decomposition of the data set would be lost.

The correlation matrix R is obtained from

$$R = Z^T Z/(N-1) \tag{3.2}$$

where R an nxn symmetric matrix.

Eq.(3.1) can be rewritten as

$$F = Z\ B \tag{3.3}$$

where

$$B = (A^T)^{-1} \tag{3.4}$$

Eq.(3.3) indicates that the i-th new variable f_i (i=1,2,...,n) is a linear combination of the original variables z_1, z_2,..., z_n, the coefficients of which are the elements of the eigenvector associated with the i-th largest eigenvalue. The variance of the new variables is

$$S_F^2 = F^T F$$

$$= B^T R B \tag{3.5}$$

According to the constraints mentioned above, S_F^2 is maximized under the condition that $BB^T = I_n$; matrix B, which is now identical to A, is orthogonal. The orthogonality of B eliminates the trivial solution for which the elements of B tend to infinity. Using the method of Lagrangian multipliers, we obtain that

$$R\,B = B\,\Lambda \tag{3.6}$$

where each column of B is an eigenvector of R, and Λ is a diagonal matrix consisting of the eigenvalues (λ_j, $j=1,2,\cdots,n$) of R in descending order.

The description of empirical orthogonal function analysis is now complete. F is referred to as the empirical orthogonal variable matrix and B as the empirical orthogonal weight matrix. From Eqs.(3.5) and (3.6), it can be seen that

$$S_F^2 = \Lambda \tag{3.7}$$

Therefore, the trace of matrix Λ equals that of matrix R. It indicates that the i-th new variable accounts for a percentage of the total variance of the original variables equal to the (i-th eigenvalue)/(trace of Λ)x100.

3.2 Principal Component Analysis

Let us now rescale the empirical orthogonal variable matrix F and empirical orthogonal weight matrix B by $\Lambda^{-1/2}$ and $\Lambda^{1/2}$ respectively to give

$$P = F\ \Lambda^{-1/2}, \tag{3.8}$$

and

$$L = B\ \Lambda^{1/2}, \tag{3.9}$$

where $\Lambda^{-1/2}$ and $\Lambda^{1/2}$ are diagonal matrices composed of $(\lambda_j)^{-1/2}$ and $(\lambda_j)^{1/2}$ $(j=1,2,\ldots,n)$ respectively. Then, P is known as the matrix of principal component and L is the matrix of principal component loading. The variance of the new variables becomes unity. The matrix P is orthonormal ($P^T P = I_n$) and

$$Z = P\ L^T, \tag{3.10}$$

$$R = L\ L^T$$

$$= B\ \Lambda\ B^T, \tag{3.11}$$

and

$$L = Z^T\ P. \tag{3.12}$$

Thus, the new variables in matrix P are uncorrelated to each other and have unit variance. But, unlike empirical orthogonal functions, the principal component loading vectors are no longer orthogonal. Therefore, the spatial patterns represented by the principal component loading vectors are not additive. To understand the meaning of the principal component loadings, it is convenient to consider matrix Z and P as being composed of n vectors, each of which has N observations. From Eq.(3.12), the principal component loading matrix is then given by the projections of the original variables onto the principal components.

The correlation matrix R has a rank n. Suppose there are only r

eigenvalues of R different from zero, then we can find a set of (n-r) orthogonal vectors onto which the projections of the z-vectors are zero.

Therefore, Eq.(3.11) becomes

$$R = L_{(r)} L_{(r)}^{T} \qquad (3.13)$$

which is able to reproduce the complete variability of the original set of time series.

3.3 Rotated Principal Component Analysis

It has been demonstrated that the unrotated solutions have some shortcomings such as domain size and shape dependence, subdomain instability and sampling errors under the condition of closely spaced eigenvalues. Also, physical interpretation is difficult when the true signal is a combination of several spatial patterns. These problems may be reduced in some cases by rotating the initial solution (Richman, 1986). The rotated solution is less domain dependent and tends to show simple structures (Thurstone, 1947). If simple structure exists in the data set, physical interpretation is easier and the underlying mechanisms dominating the complicated variations may be more easily isolated and studied.

The Varimax method, a widely used orthogonal rotation, will be applied to the initial solution in this study. The rotation of the principal component loading matrix is based upon the following equation (Richman, 1986) :

$$L^* = L\,T + E \qquad (3.14)$$

where

L = the n x r initial principal component loading matrix,

L^* = the n x r rotated principal component loading matrix,

T = an r x r transformation matrix,

and

E = an n x r residual matrix.

The transformation matrix is determined such that the trace of $E^T E$ is a minimum. For orthogonal rotation, matrix T is orthonormal (i.e. $T^T T = I_r$). Then,

$$T = (L^T L)^{-1} L^T L^* \qquad (3.15)$$

The Varimax method attempts to simplify each column of the principal component loading matrix L^* as a method for isolating the simple structure. The simplicity of a principal component is defined in terms of the variance of the squared loading of L^*

$$S = \left\{ n \sum_{i=1}^{n} (l_{ij}^{*2})^2 - \left(\sum_{i=1}^{n} l_{ij}^{*2} \right)^2 \right\} / n^2 \qquad j = 1,2,\cdots, r \qquad (3.16)$$

where n is the number of variables, r is the number of the principal component loadings submitted to rotation, and l_{ij}^* represents the rotated solution of the j-th principal component loading. The principal component loading has greatest simplicity when the S is at a maximum, and then the l_{ij}^*'s tend to be zero or one. The principal component loading vectors are rotated in pairs until S reaches a maximum. Suppose r (less than or equal to n) principal component loadings are submitted to rotation and the

resulting matrix is denoted by $L^*_{(r)}$, Eqs.(3.10)-(3.12) still hold if we substitute matrices P and L with the rotated principal component $P^*_{(r)}$ and principal component loading matrix $L^*_{(r)}$. The rotated principal component matrix can be calculated by

$$P^*_{(r)} = Z\ R^{-1}\ L^*_{(r)} \tag{3.17}$$

where the inverse of the correlation matrix R can be obtained from Eq.(3.11). In particular,

$$R^{-1} = B\ \Lambda^{-1}\ B^T. \tag{3.18}$$

Because selection rules based upon Monte Carlo techniques are computationally expensive and because of the exploratory nature of this study, the determination of the number of principal components to be subjected to rotation was made on a subjective basis.

The important properties of the rotated principal component analysis are summarized as follows:

(a) The rotated principal components are temporally orthogonal to each other, and thus the variances they explain are additive.

(b) The rotated principal component loading vectors are not spatially orthogonal so that the rotated spatial structures are not additive.

(c) The rotated solution has less domain shape and size dependence and has less subdomain instability than the unrotated solution.

(d) The rotated solution greatly reduces the sampling errors which are very severe for the unrotated solution in the case that the

eigenvalues are closely spaced.

(e) Rotated principal components do a better job of isolating simple structure in the data set

CHAPTER 4: TIME-MEAN FIELD

Before examining the transient disturbances of the jet stream, it is worthwhile to examine the seasonal-mean flow in which the wind fluctuations are embedded. The 200mb seasonal-mean rotational zonal wind field, $\bar{u}_\psi$ is shown in Fig. 4.1.(a). The well-known East Asia jet stream is centered at about 33°N, 140°E with maximum wind speed about 65ms^{-1}; easterlies prevail in the tropical region south of about 15°N. The 200mb divergent component of the mean meridional wind ($\bar{v}_\chi$; Fig. 4.1.(b)) is more complicated. In the East Asia winter monsoon region, the southerlies increase rapidly from the equator to a maximum at about 7°N, decrease northward to a minimum at about 20°N, increase again to a secondary maximum at about 30°N, and then decrease northward to a minimum at about 40°N. North of 45°N, northerly winds prevail and reach a maximum at about 55°N. It is noteworthy that, in the midlatitude jet entrance region, the implied vertical circulation is such that there is maximum sinking motion north of 30°N and rising motion near 25°N which is far away from the tropical convection region. The locations of these vertical motion centers suggest a dynamical relationship with the large wind accelerations.in the jet entrance region. This thermally direct circulation would also convert available potential energy into kinetic energy as proposed by Pan and Zhou (1985), and Blackburn (1985). The large gradient of the divergent meridional wind, especially in the tropical region

between 95°E and 130°E where the maritime continents are located, is consistent with the strong convection normally found over this area in wintertime. Over the northern China and Siberia (50–55°N, 110–120°E), the strong negative gradient implies strong sinking motion in association with the Siberian high. The implied seasonal mean vertical circulation over the entire region can therefore be characterized as a local Hadley circulation with rising motion over equatorial maritime continental region and sinking motion centered over northern China and Siberia with a superimposed thermally direct circulation confined within 20–40°N as suggested by Pan and Zhou (1985).

According to the confluence theory of Namias and Clapp (1949), the stationary jet stream is maintained by the steady-state cross-isobar (ageostrophic) flow at the jet stream level; the transient eddies play a relatively unimportant role. According to this theory, the momentum balance in the entrance region of the stationary jet stream can be formulated as follows:

$$\frac{\partial \bar{u}}{\partial t} \cong f\bar{v}_a - \bar{u}\frac{\partial \bar{u}}{\partial x} - \bar{v}\frac{\partial \bar{u}}{\partial y} \cong 0 \qquad (4.1)$$

where

$$\bar{v}_a = \bar{v} - \bar{v}_g \cong \bar{v}_\chi$$

f = Coriolis parameter

Eq.(4.1) states that the strong westerly momentum flux advection is balanced by the Coriolis force acting on the meridional ageostrophic flow. The steady-state cross-isobar wind can be

approximated by the mean meridional component of the divergent wind. In the jet entrance region, the advective momentum is estimated to be on the order of $30ms^{-1}$ per day, hence the ageostrophic wind has to be poleward and on the order of $3ms^{-1}$ to account for the observed acceleration of air as it approaches the jet stream (Wallace, 1978). The magnitude of the maximum southerly wind near $30^{o}N$ in Fig. 4.1.(b) is in good agreement with the estimated value. This supports the assertion that the eddy activity is secondary effect.

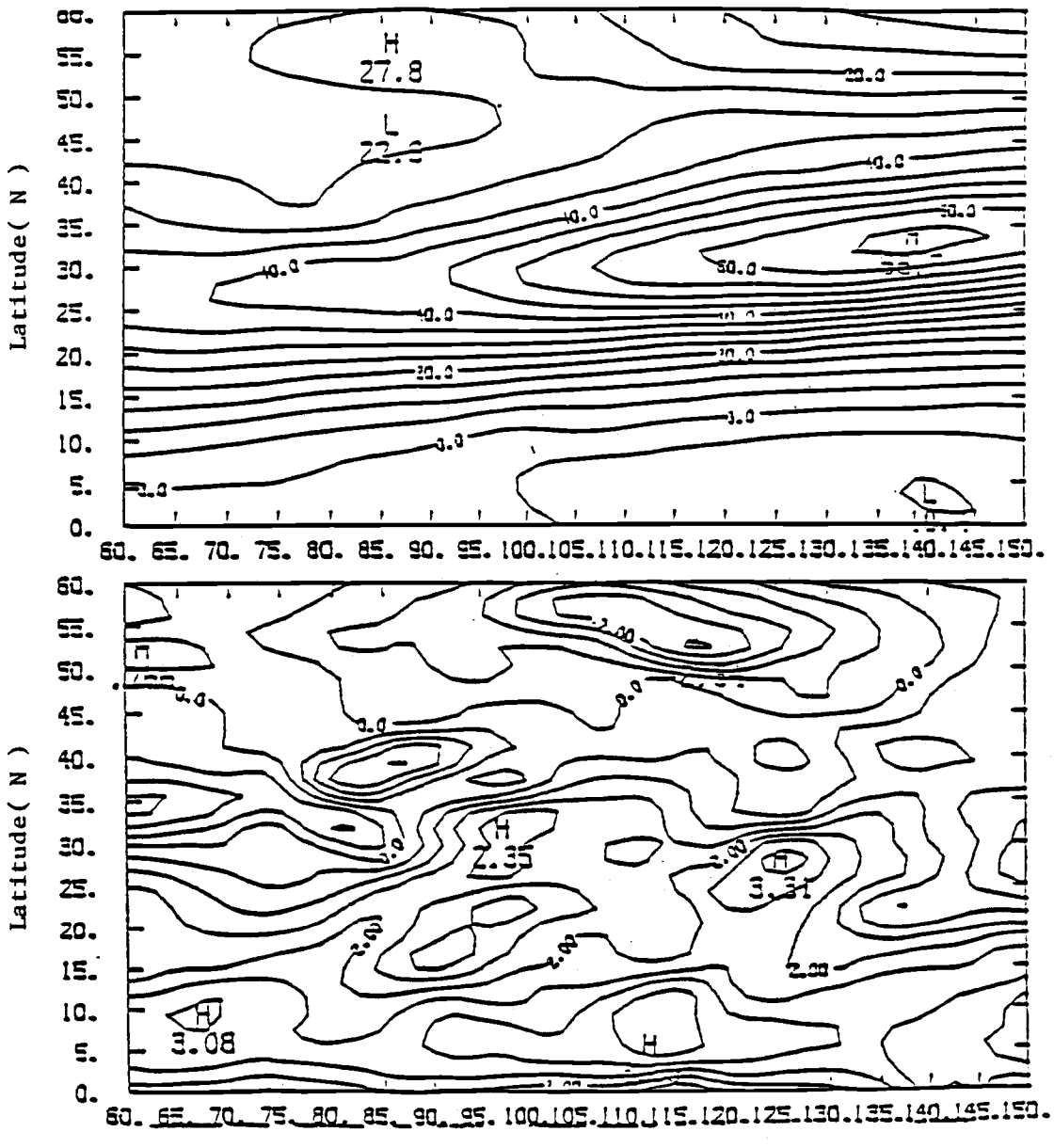

Fig.4.1 (a) Time-mean state of 200mb rotational zonal wind and (b) 200mb divergent meridional wind. Unit: ms^{-1}.

CHAPTER 5: RESULTS AND DISCUSSIONS

5.1 Rotated Principal Component Analysis

The principal component analysis is applied to (A) the transient part of the zonal component of the rotational wind (u_ψ'), (B) the transient part of the meridional component of the divergent wind (v_χ'), and (C) a linear combination of the rotational and divergent wind components used in (A) and (B). In each case, the spatial domain extends over 0–52.5^{o}N, 97.5–150.0^{o}E with a grid interval of 7.5 degree in both zonal and meridional directions. There are 64 spatial grid points and 180 analysis times. The reason for analyzing the combined data set (C) is to find the concurrent patterns of variability in the jet stream and the meridional divergent wind.

The data matrix Z for (A), (B), and (C) are shown as follow:

(A) $Z = [\ \hat{u}_{\psi,1},\ \hat{u}_{\psi,2},\ \cdots,\ \hat{u}_{\psi,63},\ \hat{u}_{\psi,64}\ ]$

(B) $Z = [\ \hat{v}_{\chi,1},\ \hat{v}_{\chi,2},\ \cdots,\ \hat{v}_{\chi,63},\ \hat{v}_{\chi,64}\ ]$

(C) $Z = [\ \hat{u}_{\psi,1},\ \hat{u}_{\psi,2},\ \cdots,\ \hat{u}_{\psi,63},\ \hat{u}_{\psi,64},\ \hat{v}_{\chi,1},\ \hat{v}_{\chi,2},\ \cdots,\ \hat{v}_{\chi,63},\ \hat{v}_{\chi,64}\ ]$

where $\hat{u}_{\psi,j}$ and $\hat{v}_{\chi,j}$ ($j = 1, 2, \cdots, 63, 64$) are column vectors with length 180.

The first five components obtained from (A), (B) and (C) were

found to be able to represent the most prominent features in the time-latitude and time-longitude cross-sections of u_ψ' and v_χ' (see Section 5.2). The percentage of variance explained by the first five eigenvectors is listed in Table 5.1. The first five principal component loading vectors were submitted to Varimax rotation and the associated rotated principal components (time series of amplitude) were computed according to Eq.(3.17). Spatial structures of the rotated principal component loading vectors were examined subjectively by contouring the values in space. In the following discussion the spatial patterns are presented for positive amplitude.

(A) u_ψ'

The first interesting mode as shown in Fig. 5.1.a is characterized by a dipole-type pattern over the entrance region of the stationary jet stream. A maximum westerly anomaly appears over the East China Sea and the southern tip of Japan, and a minimum of smaller magnitude appears over northern China. For positive amplitude this mode intensifies the jet stream to the south and weakens it to the north so that the jet stream shifts southwestwards. The associated time series of the amplitude (principal component) is shown in Fig. 5.1.b.

The second mode shown in Fig. 5.2 is, to some degree, similar to the first mode with a large maximum easterly anomaly in the north and a maximum westerly anomaly located to the south. The reconstructed field of the first two modes (Fig. 5.3) shows a

typical disturbance that slowly propagates eastwards and somewhat southwards. The westerly anomaly intensifies when it moves from East Asia coast into western Pacific and then decays when it moves further eastwards. This slowly eastward-moving disturbance is embedded in the jet stream and can be called jet streak.

(B) v_χ'

The first mode (Fig. 5.4.a) is characterized by two pairs of dipole-type patterns which are out of phase with each other. One is in the western part of the domain near 105°E with a maximum southerly anomaly at about 15°N and a maximum northerly anomaly at 37.5°N. This implies a thermally direct vertical circulation with strong rising motion in the tropical region, intense sinking motion in the region of 15–30°N, and a thermally indirect vertical circulation with rising motion north of 37.5°N and sinking motion in the region of 30–37.5°N. When the amplitude of this mode is positive, we would expect the tropical convection to be enhanced and the sinking motion of Siberian high to be reduced (Pan and Zhou, 1985). The second dipole is in the eastern part of the domain near 140°E with a maximum southerly anomaly at 15°N and maximum northerly anomaly at about 35°N. The implied vertical circulation is thermally indirect south of about 25°N and thermally direct to the north.

The first modes of u_ψ' and v_χ' appear to be related to the pairs of anomalous cyclonic and anticyclonic centers that were found to

propagate through the wintertime East Asia jet stream by Pan and Zhou (1985) and Pan (1987). Note that the amplitudes of $u_\psi'$and v_χ'(Fig. 5.4.b) appear to be correlated with little lag. This correlation is confirmed by cross-spectral analysis (Fig.5.4.c; see Appendix for details) showing that these two time series are well-correlated near the frequency of 1/15 (day^{-1}) with the v_χ' field lagging the u_ψ' field by about 1.5 days. Thus, similar to the stationary jet stream, there exists a thermally direct circulation in the entrance region of the westerly jet streak and a thermally indirect circulation in the exit region. For an easterly jet streak, the associated secondary circulation would be thermally indirect in the entrance region and thermally direct in the exit region. The balance of forces in the jet streak will be discussed in the next section.

For negative amplitude, the first mode of v_χ' would imply that sinking motion and suppressed convective activity over the tropical maritime continent region is associated with ascending motion over central China and descending motion over northern China. The resulting enhancement of the Siberian high in northern China might trigger the winter monsoonal cold surges over East Asia (Pan, 1987). At the same time, the jet stream would intensify to the north, prior to the onset of cold surge. After the cold surge, the local Hadley circulation should be enhanced due to the upper-level increased divergence over the tropics and the convergence over central China.

The second mode of v_χ' is shown in Fig. 5.5. The pattern is characterized by a maximum southerly anomaly over southern Philippines (5–10°N, 120–130°E) and a maximum northerly anomaly over North Korea. This mode, different from the mode shown in Fig. 5.4.a which has maximum variation far away from the equatorial region, has maximum variation over the tropical region. This indicates that the second mode is related to the variation of the local Hadley circulation.

(C) Combined u_ψ' and v_χ'

The spatial structures of u_ψ' and v_χ' for the first mode obtained from the combined data set are shown in Figs. 5.6.a and 5.6.b. As expected, the westerly (easterly) jet streak is associated with a thermally direct (indirect) circulation in the entrance region and a thermally indirect (direct) circulation in the exit region. The associated principal component is shown in Fig. 5.6.c.

The second mode shown in Fig.5.7 appears to represent the variation of local Hadley circulation. Fig. 5.7.a implies that there is a convergence center located near the center of the domain. Therefore, strengthened tropical convection is likely to be associated with an intensified local Hadley circulation. The rotated principal component (Fig. 5.7.c) indicates that the variation of the local Hadley circulation due to eastward-propagating long-synoptic waves may be quite large.

eigen-vector	percentage of variance		
	A	B	C
1	29.3	25.4	21.1
2	20.2	20.0	17.3
3	14.3	15.2	13.6
4	10.2	11.8	10.4
5	8.5	6.8	7.5
total	82.5	79.2	69.9

Table 5.1 The percentage of variance of the first five eigenvectors

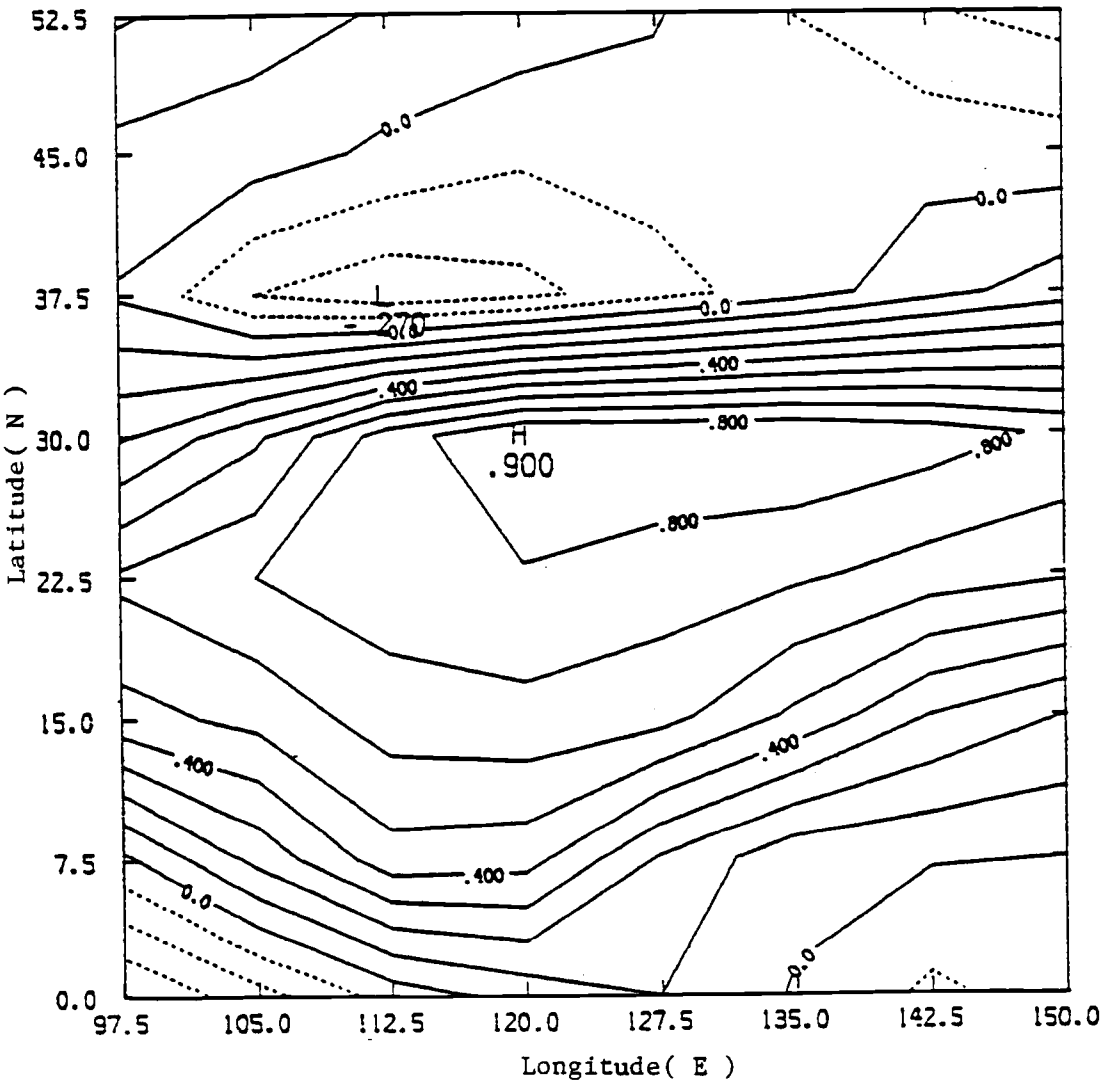

Fig.5.1.a Contours in space of the first mode of rotated principal component loading of u'_{ψ}.Day 1 corresponds to December 1, 1978.

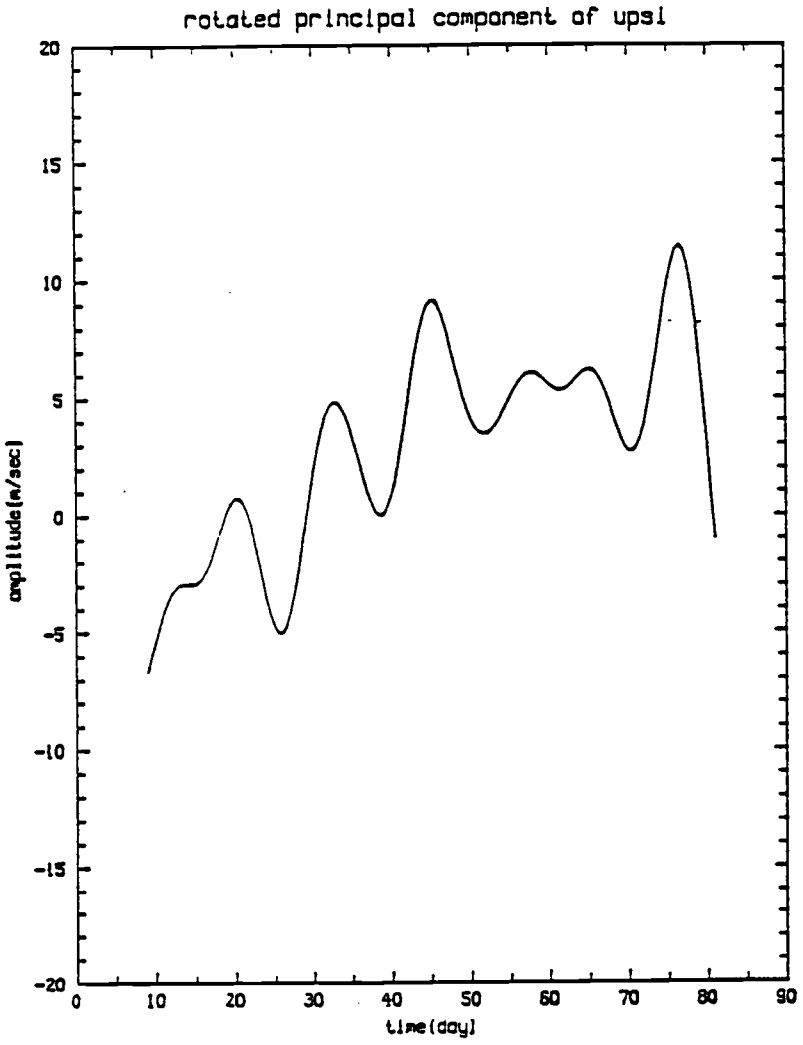

Fig.5.1.b The rotated principal component associated with Fig.5.1.a

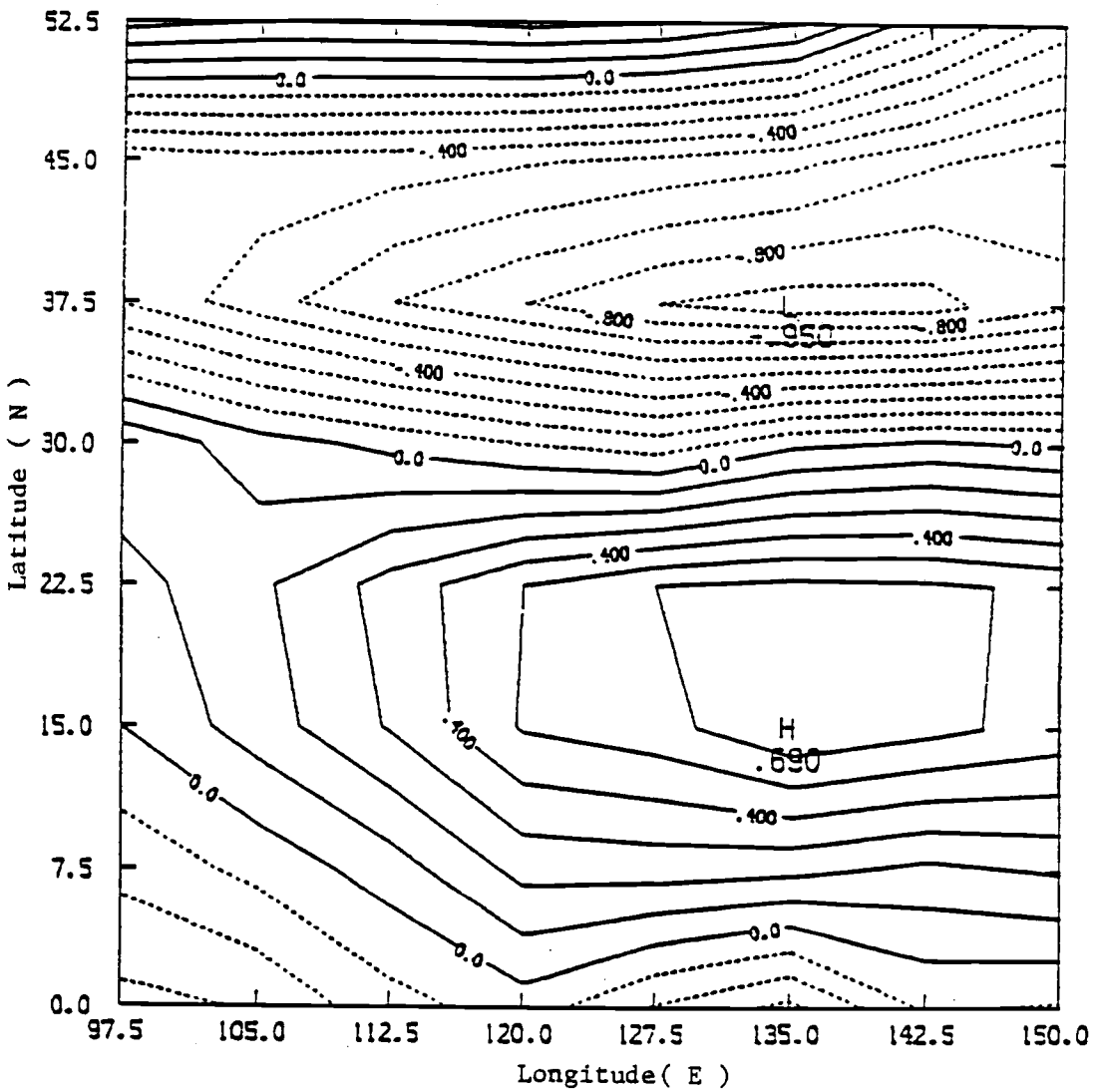

Fig.5.2 As in Fig.5.1.a except for the second mode

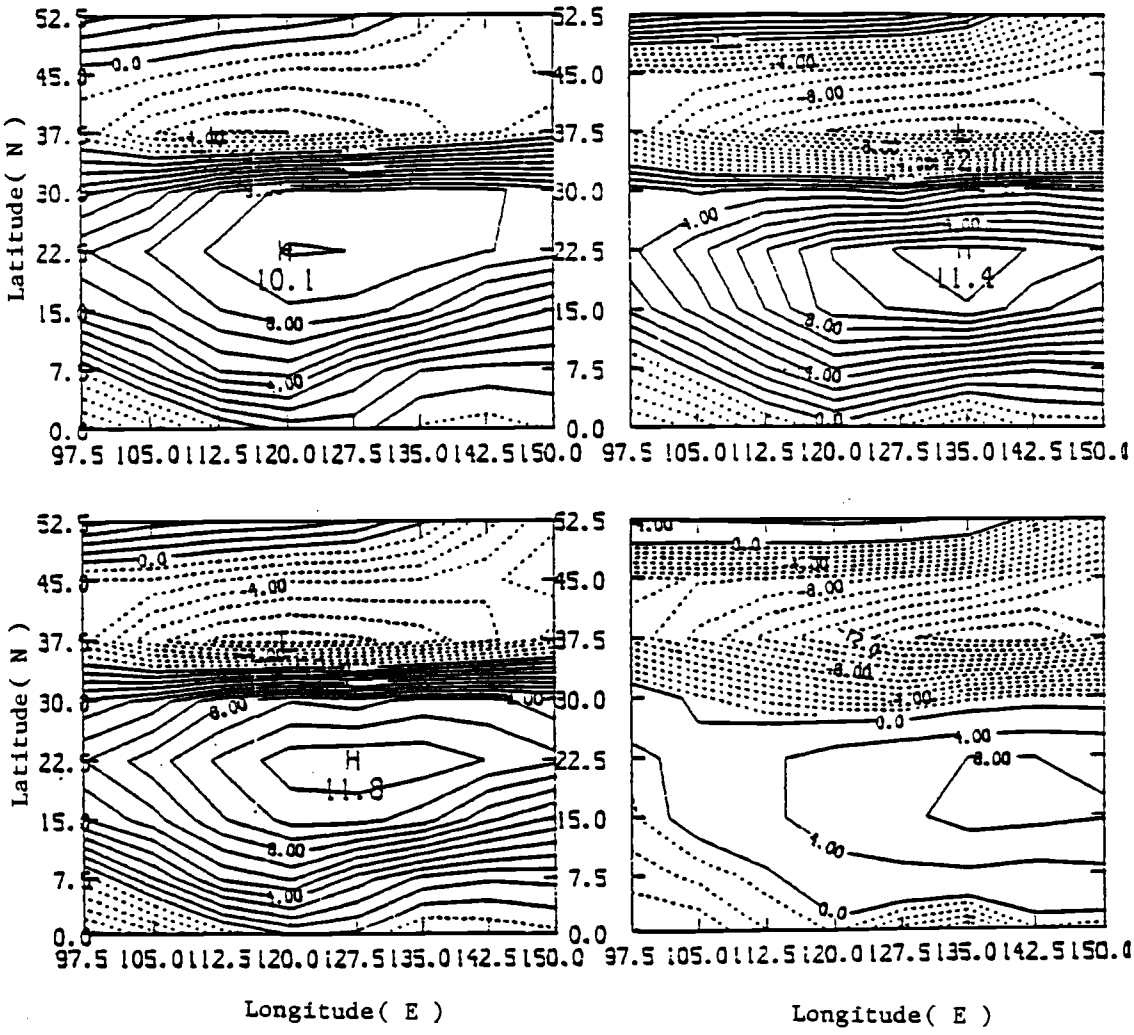

Fig.5.3 The reconstructed field from the first and second modes of u'_ψ for day 76 (February 14, 1979; upper left), day 78 (lower left),day 80 (upper right), and day 82 (lower right). Units:ms^{-1}.

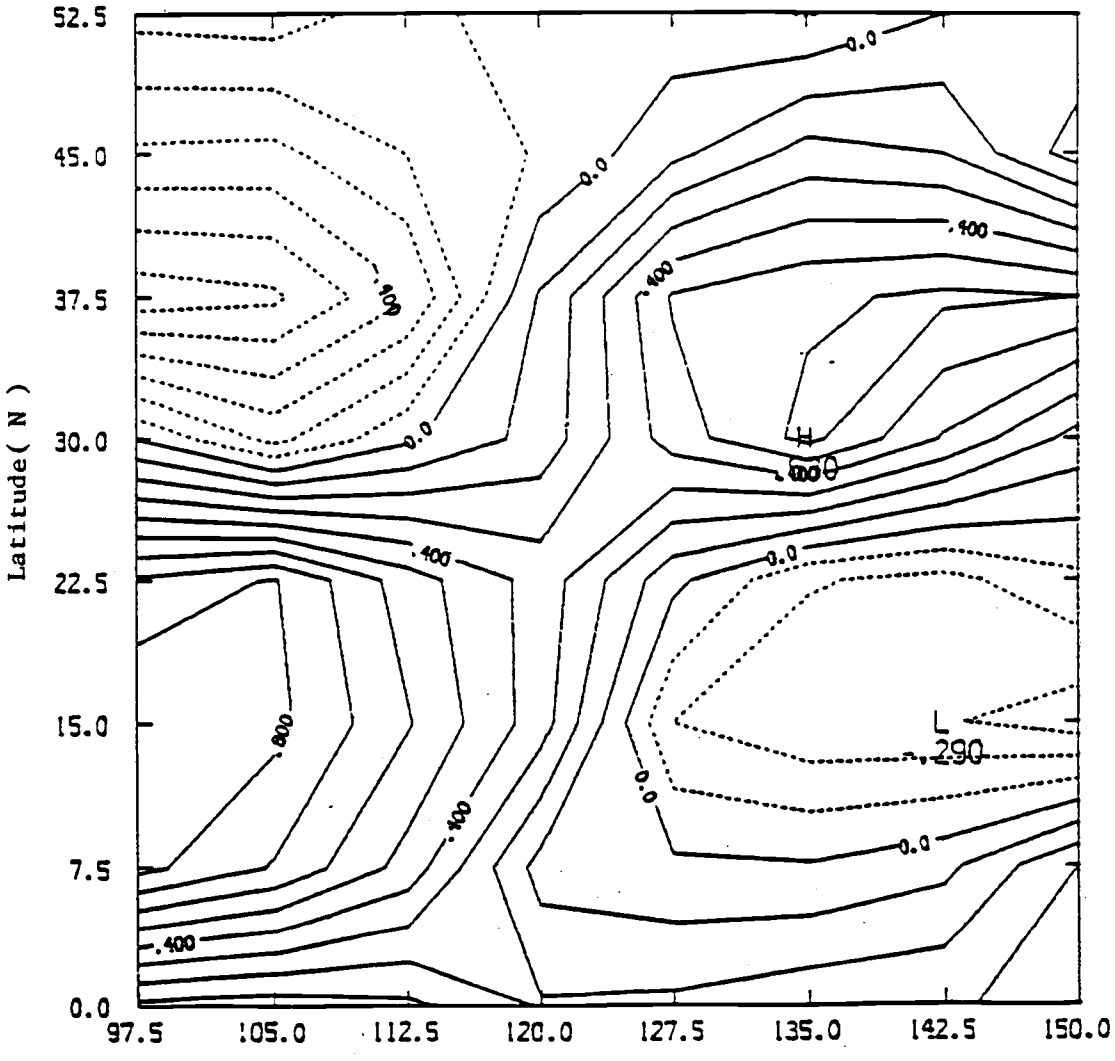

Fig.5.4.a Contours in space of the first mode of rotated principal component loading of v'_χ.

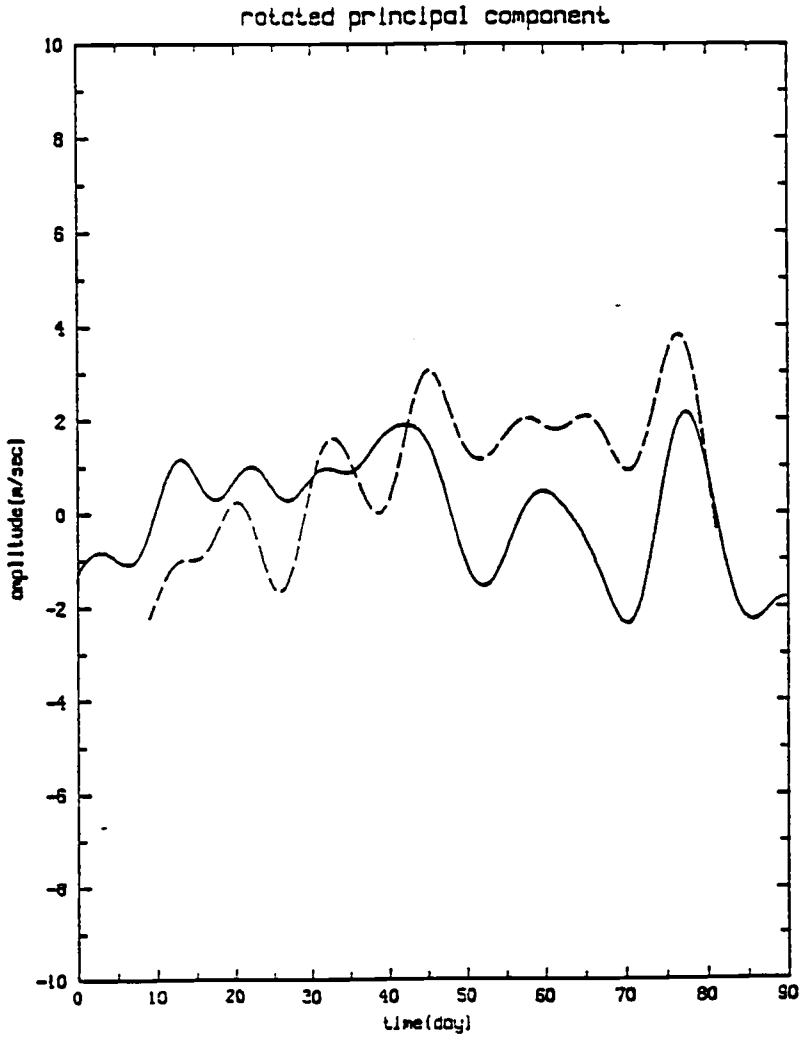

Fig.5.4.b The principal component associated with Fig.5.4.a (solid line) and that associated with Fig.5.1.a (dashed line).

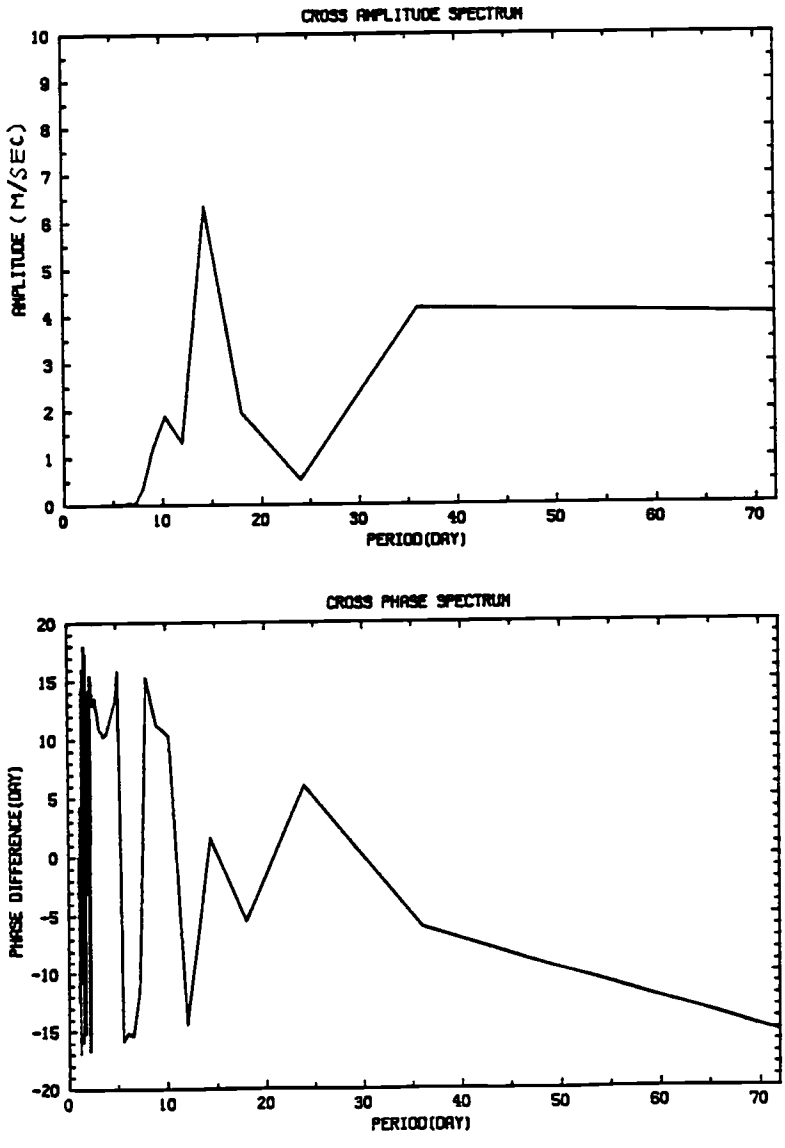

Fig.5.4.c The cross-amplitude spectrum (top) and the phase spectrum (bottom) of the two time series shown in Fig.5.4.b

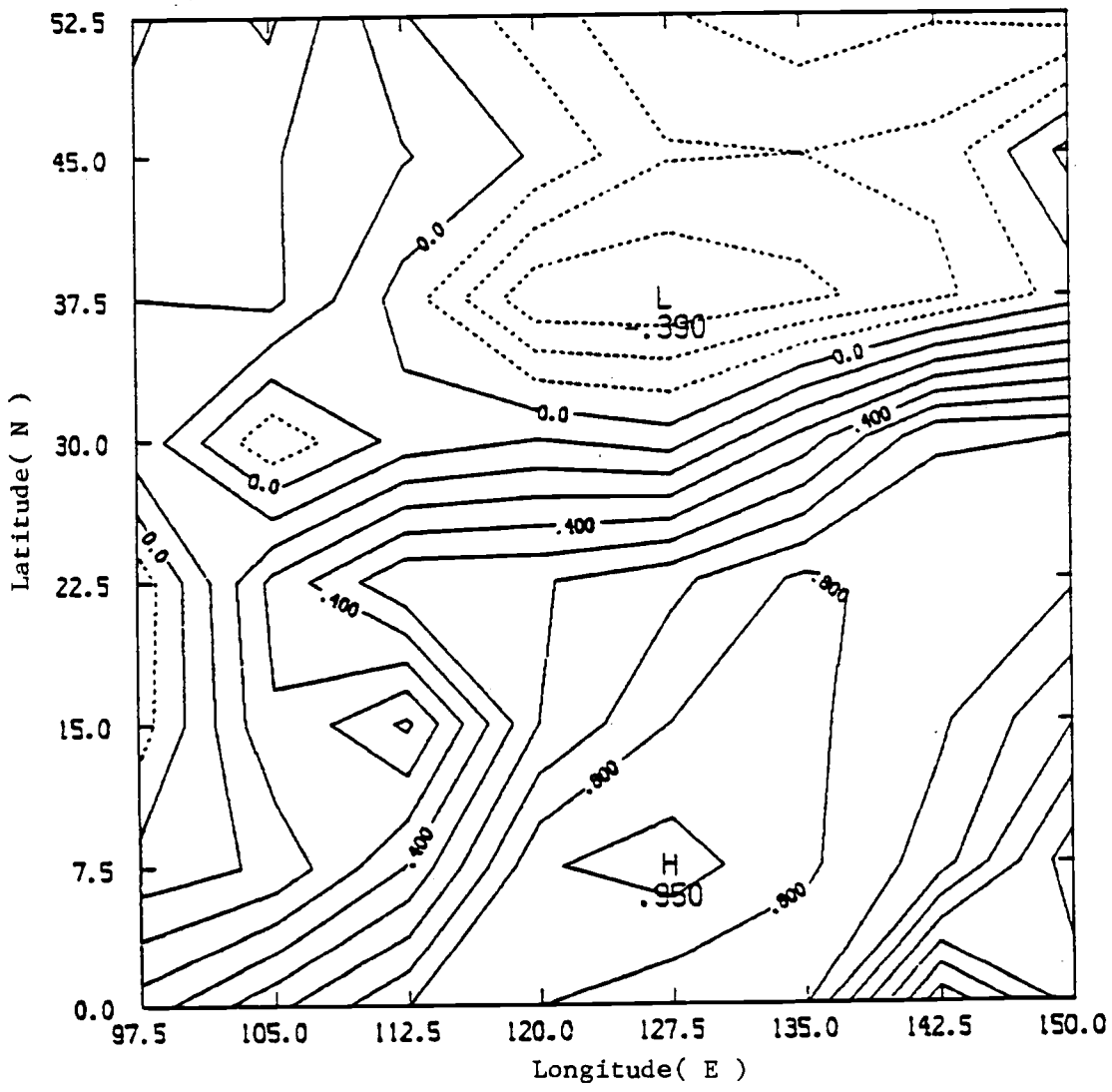

Fig.5.5 As in Fig.5.4.a except for the second mode

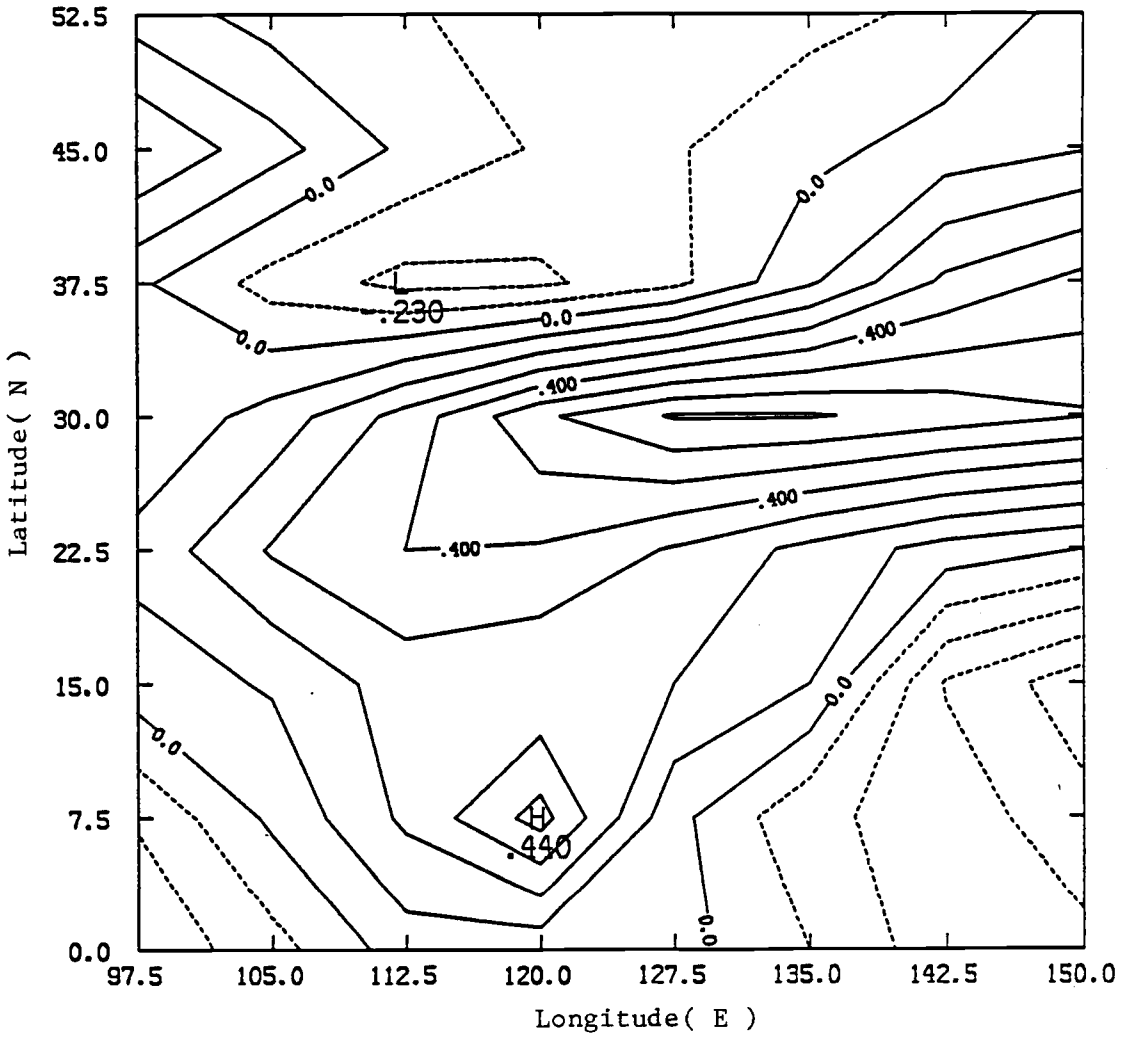

Fig.5.6.a Contours in space of the first mode of rotated principal component loading associated with u'_ψ obtained from the combined data set.

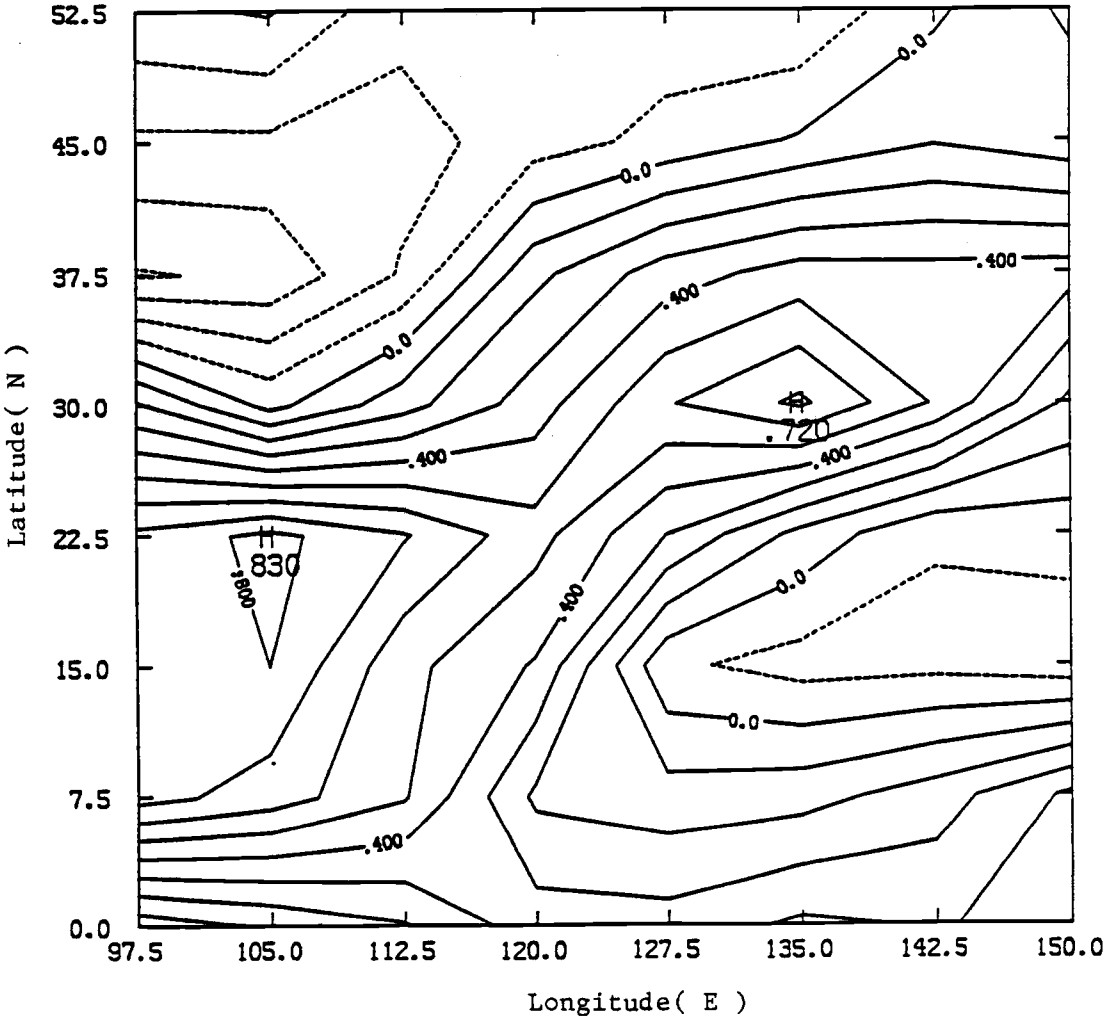

Fig.5.6.b As in (a), except for v'_{χ}.

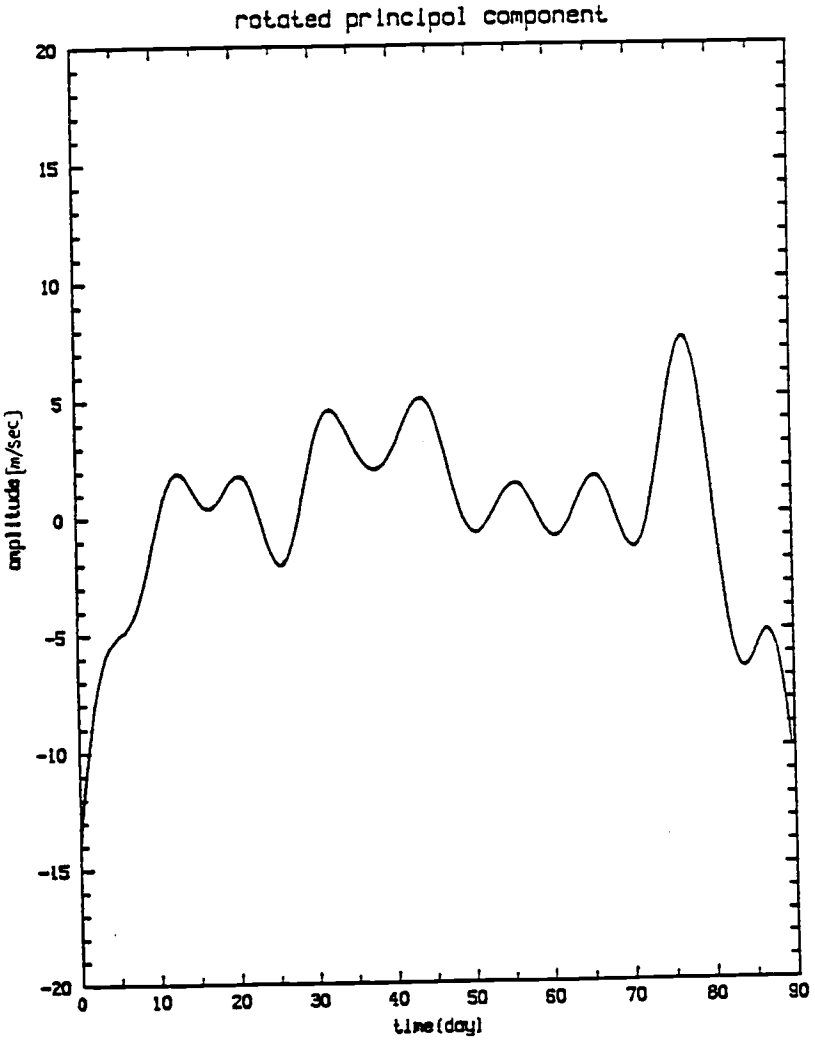

Fig.5.6.c Rotated principal component associated with Fig.5.6.a and Fig.5.6.b

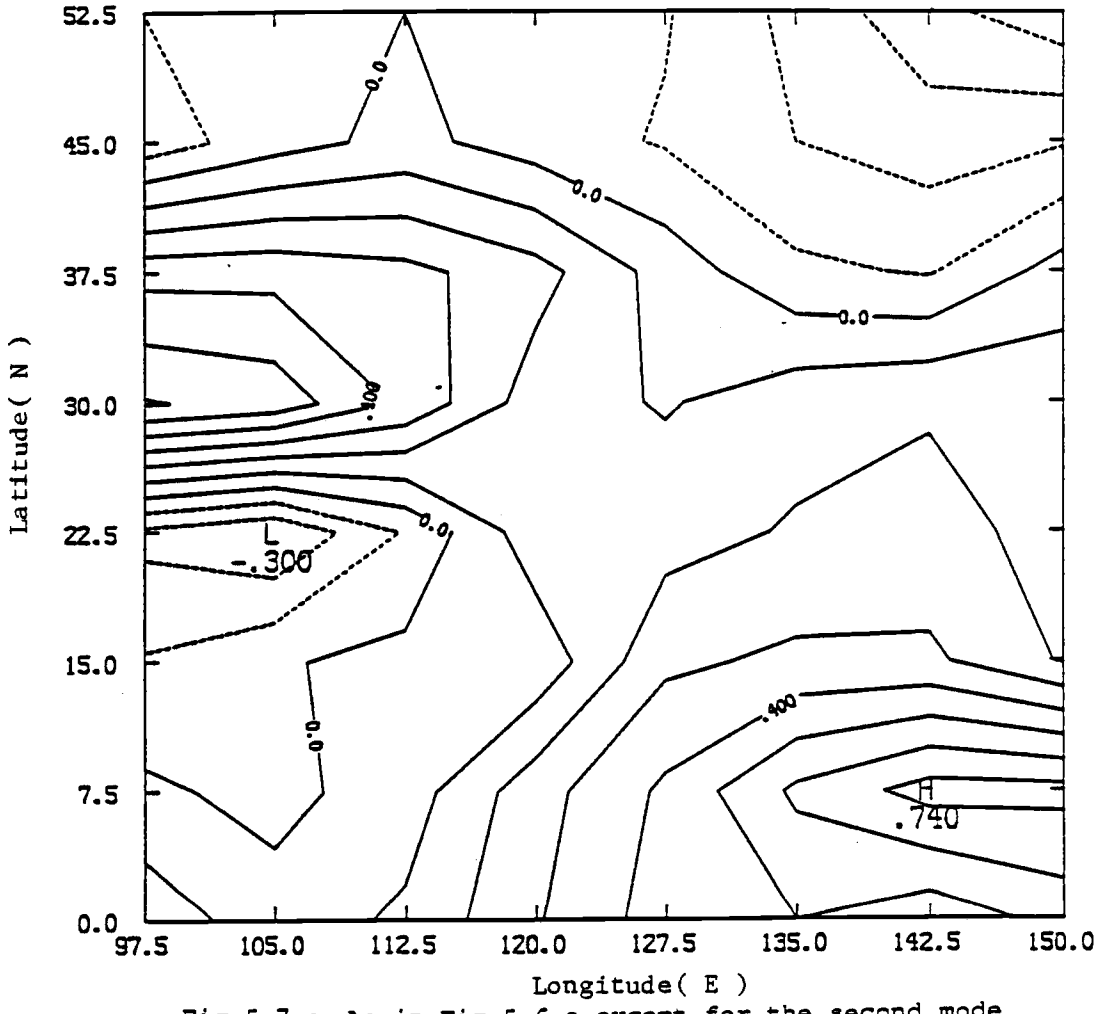

Fig.5.7.a As in Fig.5.6.a except for the second mode

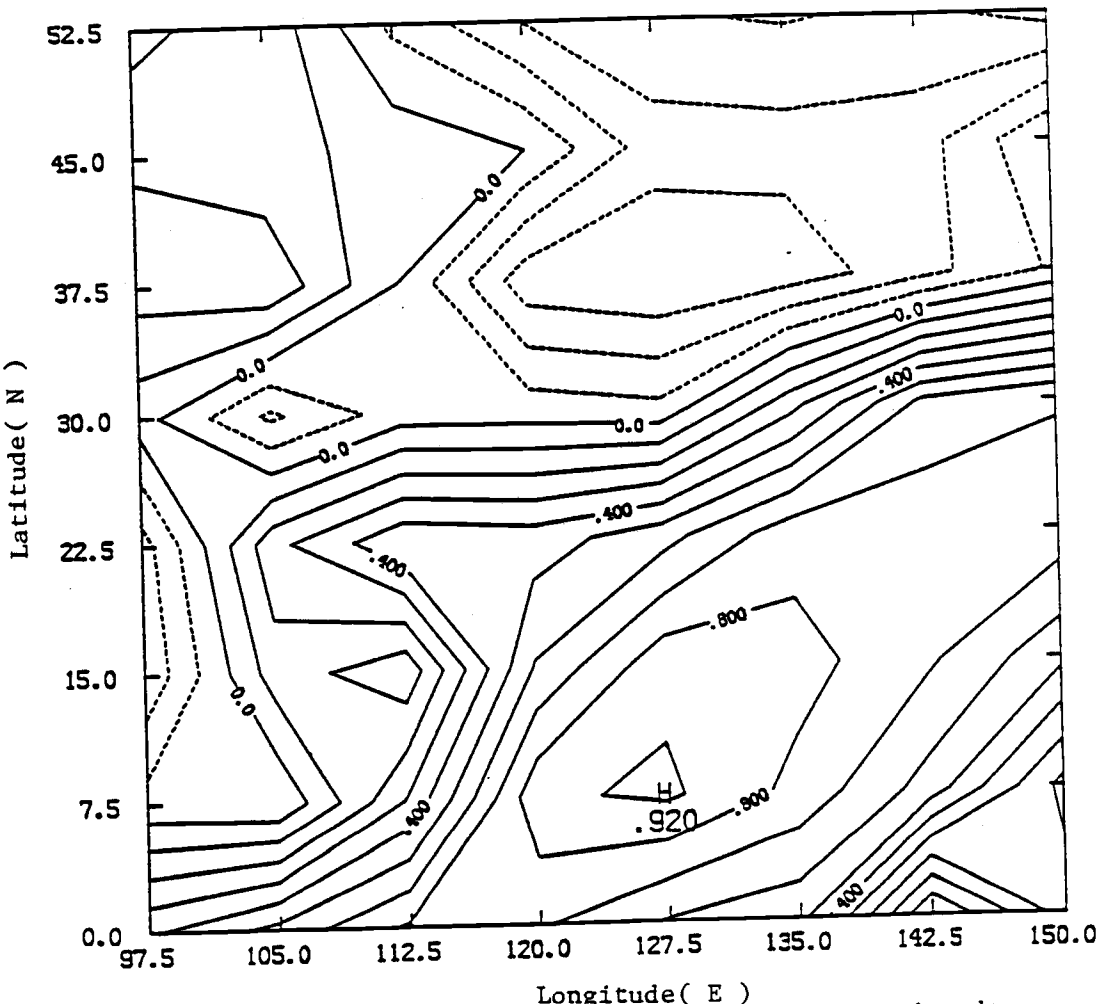

Fig.5.7.b As in Fig.5.6.b except for the second mode

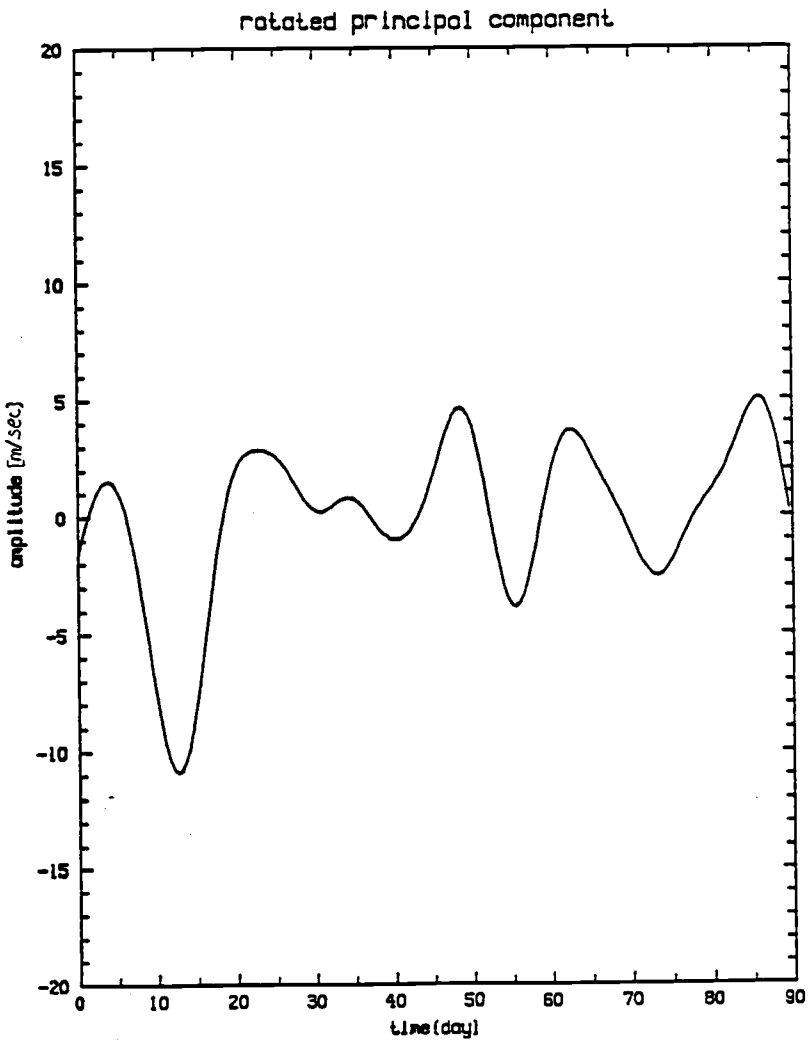

Fig.5.7.c As in Fig.5.6.c except for the second mode

5.2 Cross-Sections

To compare the jet streaks identified through rotated principal component analysis with the variability of the total field in the vicinity of the jet stream, cross-sections of rotational zonal wind u_ψ' and meridional divergent wind v_χ' were constructed. The data in Figs. 5.8 - 5.16 are time-mean removed and low-pass filtered with a cutoff period of 10 days.

The time-latitude cross-sections of v_χ' along 105^oE, 127.5^oE and 138.75^oE (Figs. 5.8 -5.10) show that there are periodic pairs of disturbances consisting of a maximum southerly anomaly in the south (north) and a maximum northerly anomaly in the north (south) over the latitude belt of $10-40^oN$. These features can be seen in the rotated principal component loading vectors shown in Figs.5.4.a and 5.6.b. There are also v_χ' variations in the equatorial region which may reflect variations of the intensity of tropical convection. This equatorial variability is captured by the mode shown in Fig. 5.5.

The time-latitude cross-sections of u_ψ' along 112.5^oE and 138.75^oE (Figs.5.11 and 5.12) are also characterized by the periodic appearance of pairs of disturbances composed of a maximum westerly anomaly in the south (north) and a maximum easterly anomaly in the north (south). The tilt of the axis of the

anomaly suggests that the u_ψ' disturbances propagate towards the jet stream region from the south and north respectively. This feature is also well-described by the principal component loading shown in Fig. 5.1.a.

The time-longitude cross-sections of u_ψ' along 26.25^oN and 33.75^oN (Figs. 5.13 and 5.14) which are mostly out of phase indicate that there are frequent pair-like eastward-propagating disturbances especially in the second half of the winter. Occasionally there are also non-propagating features (e.g. day 12). The time-longitude cross-sections of v_χ' along 15^oN and 33.75^oN (Figs. 5.15 and 5.16) also indicate there are eastward-propagating disturbances.

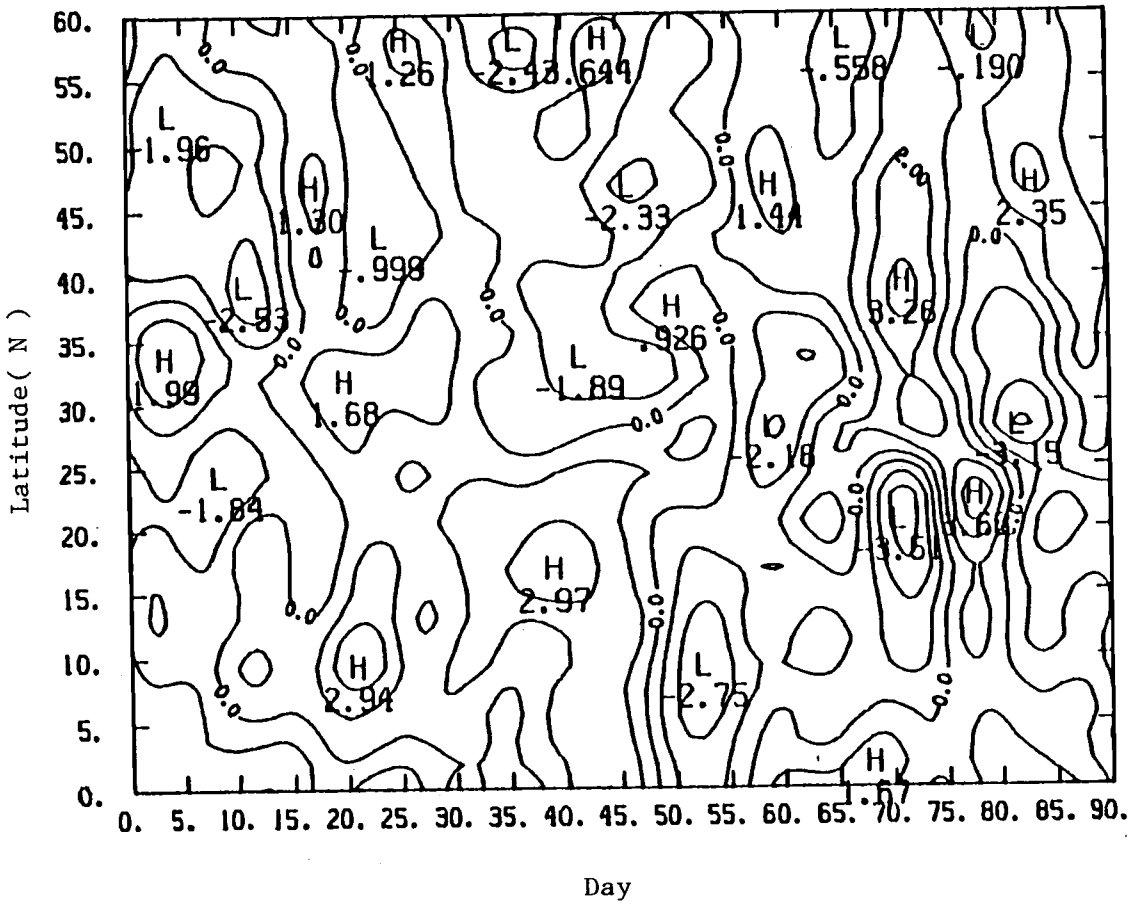

Fig.5.8 Time-latitude cross-section of v_χ' along 105°E.
Units:ms^{-1}. Day 1 corresponds to December 1, 1978.

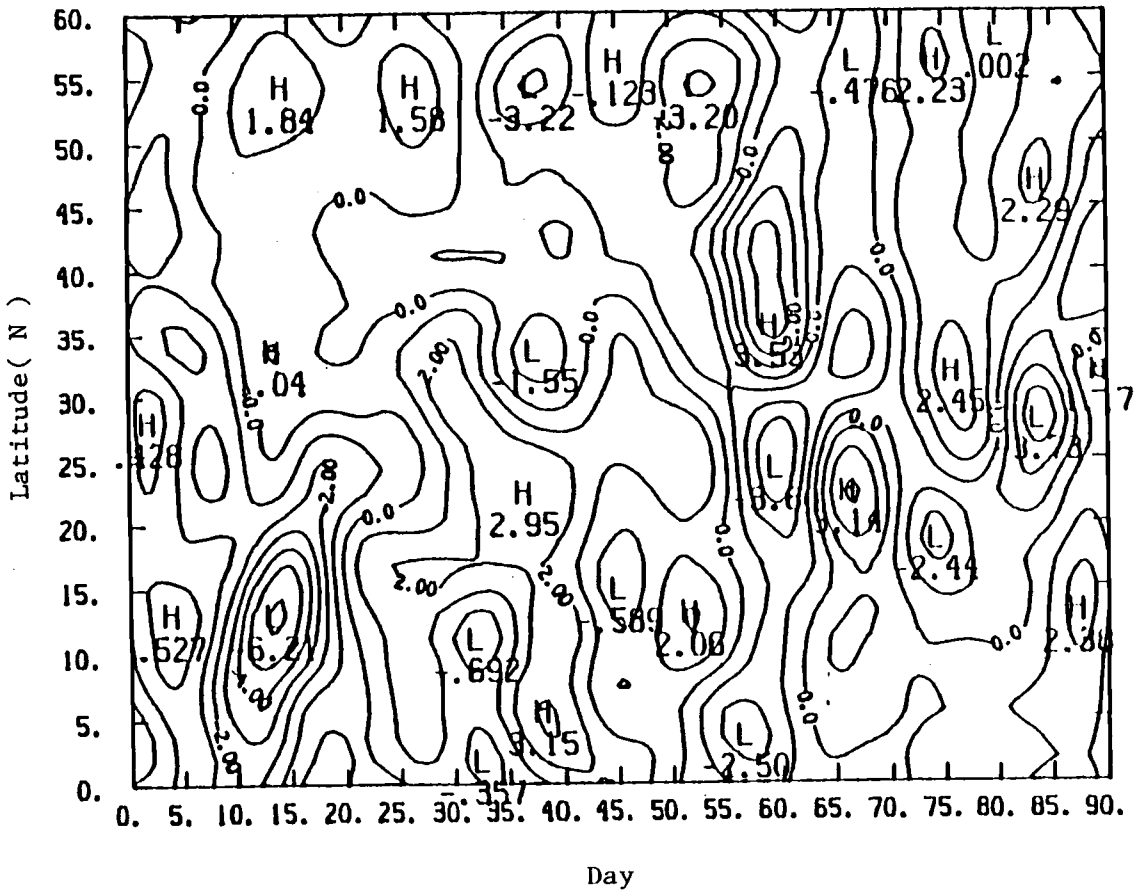

Fig.5.9 As in Fig.5.8 except for along 127.5°E.

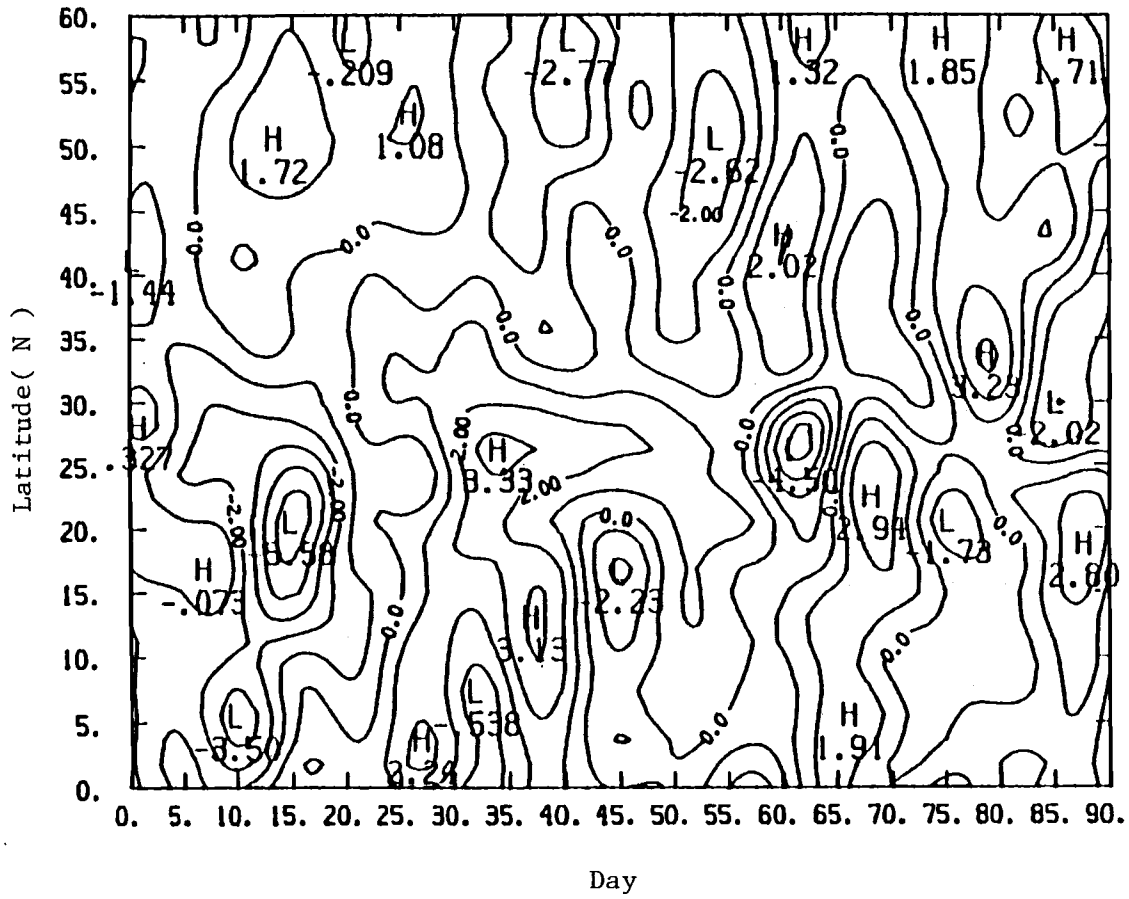

Fig.5.10 As in Fig.5.8 except for along 138.75°E.

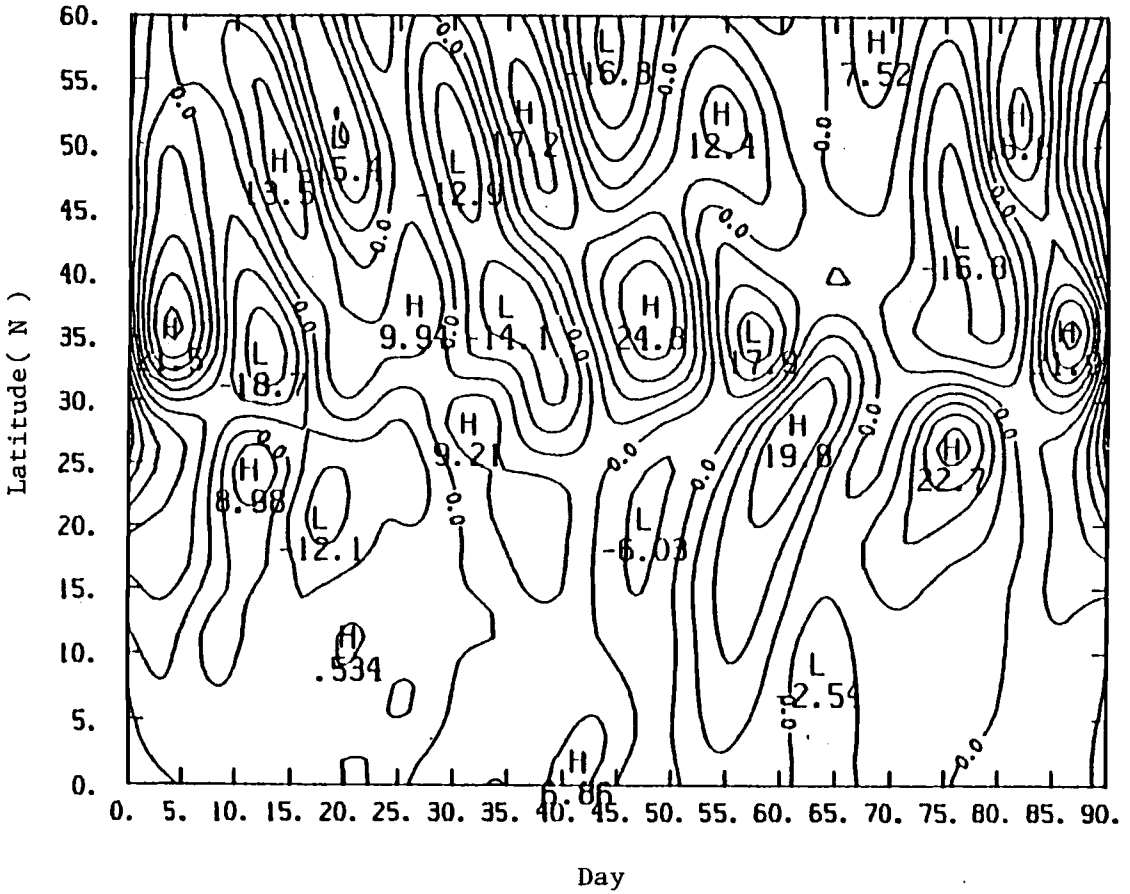

Fig.5.11 Time-latitude cross-section of u'_ψ along 112.5°E. Unit:ms^{-1}. Day 1 corresponds to December 1, 1978.

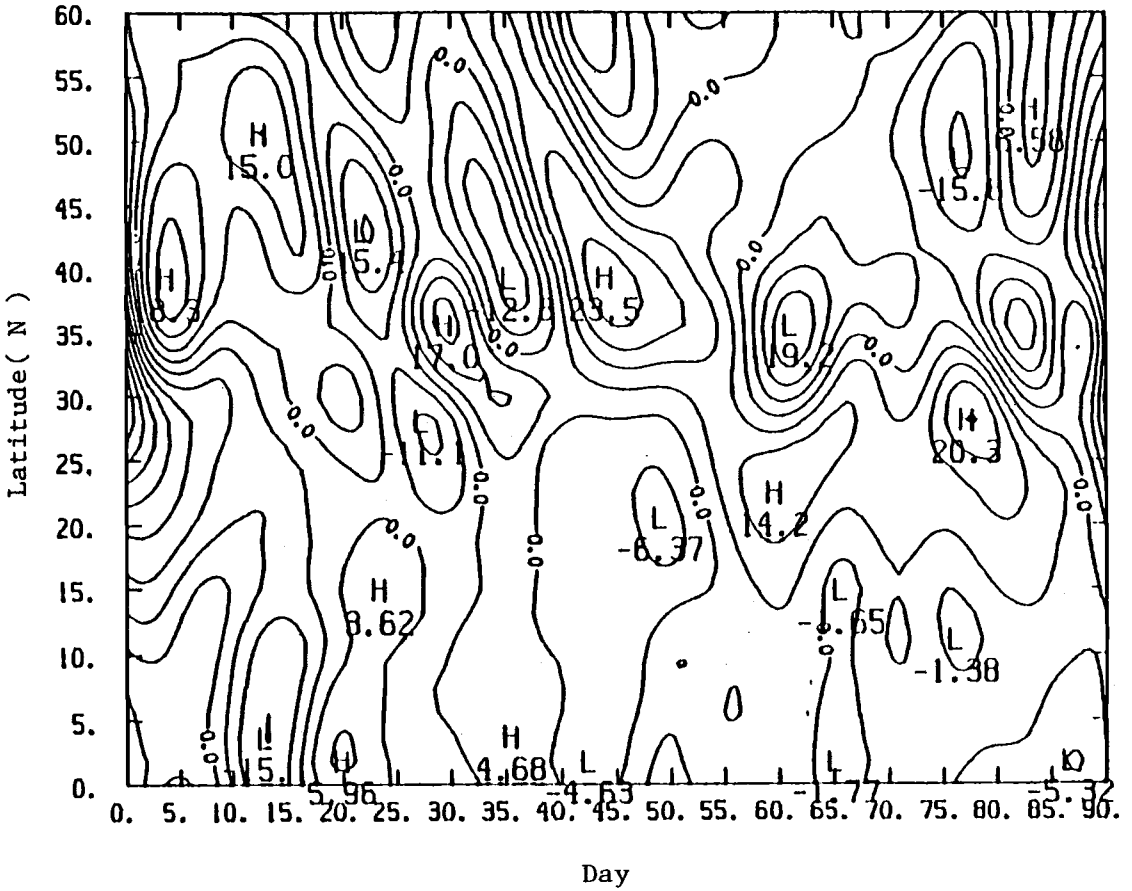

Fig.5.12 As in Fig.5.11 except for along 138.75°E.

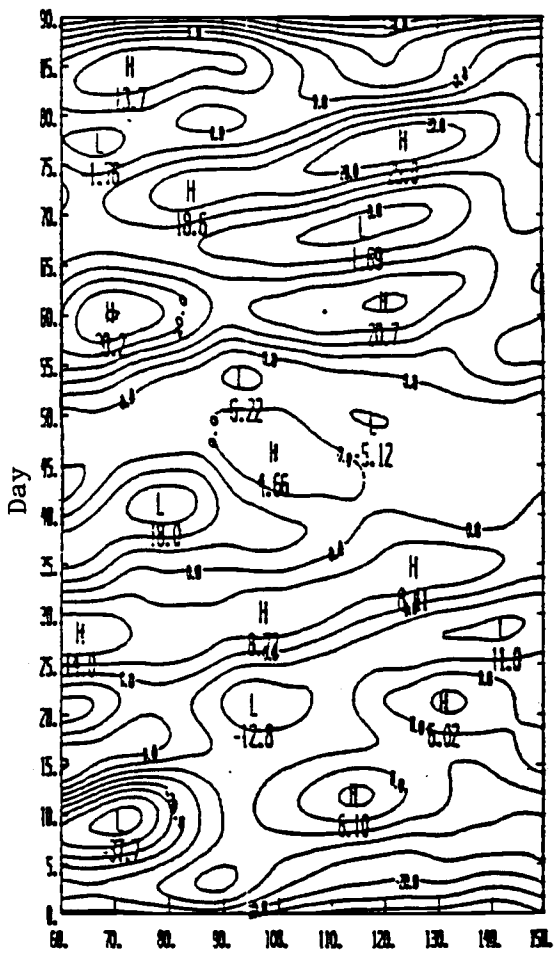

Fig.5.13 Time-longitude cross-section of u'_ψ along 26.25°N. Unit: ms^{-1}. Day 1 corresponds to December 1, 1978.

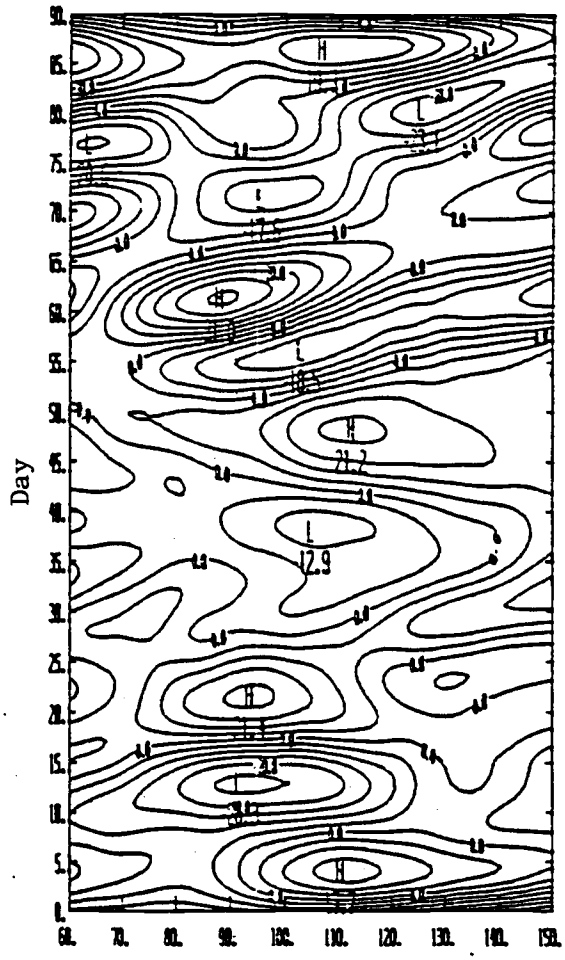

Fig.5.14 As in Fig.5.13 except for along 33.75°N

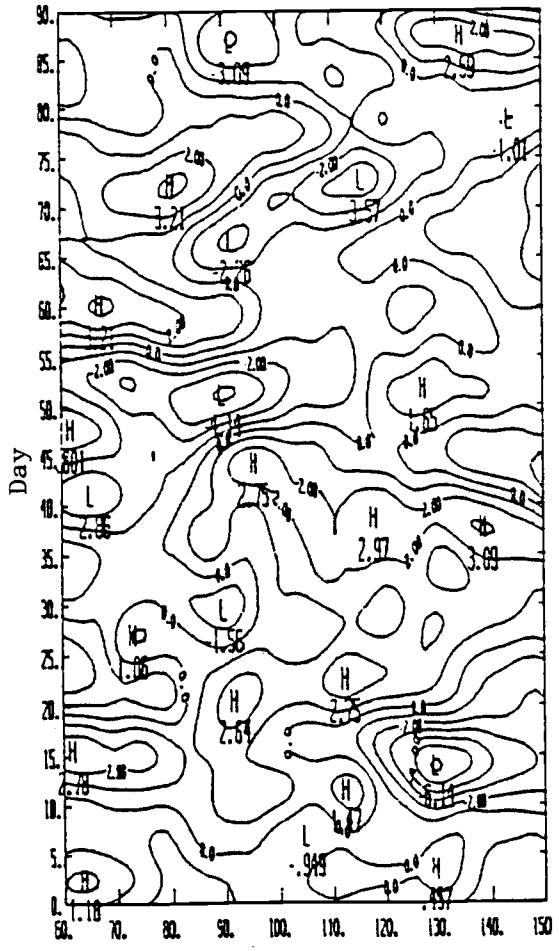

Fig.5.15 Time-longitude cross-section of v_χ along 15.0°N.Unit-ms^{-1}. Day 1 corresponds to December 1, 1978.

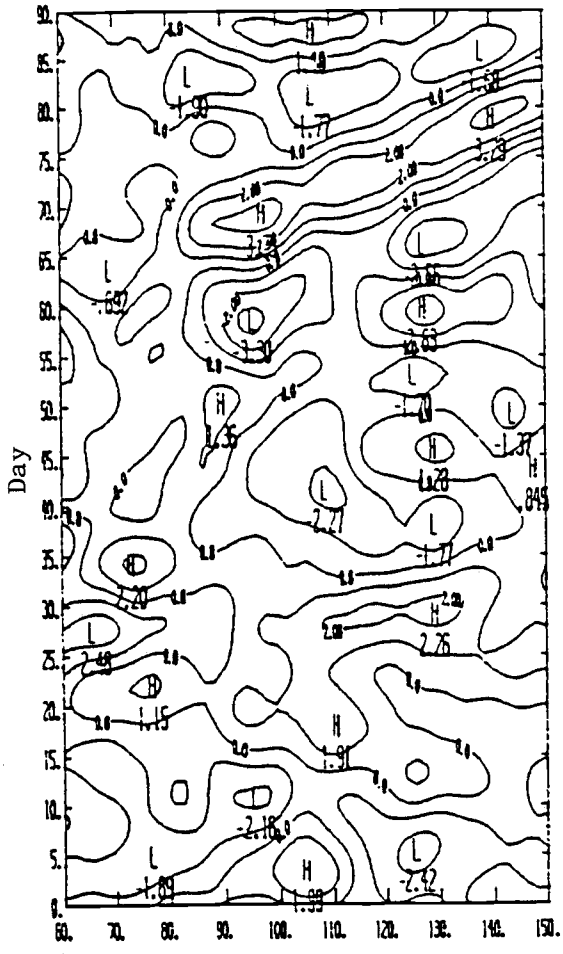

Fig.5.16 As in Fig.5.15 except for along 33.75°N

CHAPTER 6: MOMENTUM EQUATION

Since the axis of jet stream is approximately zonal, the acceleration in the entrance region is governed by

$$\frac{du}{dt} = f (v - v_g) \tag{6.1}$$

where

$$\frac{d}{dt} = \frac{\partial}{\partial t} + u\frac{\partial}{\partial x} + v\frac{\partial}{\partial y}$$

The wind can be decomposed into stationary and transient part

$$u = \bar{u} + u'$$

$$v = \bar{v} + v' \tag{6.2}$$

where bar denotes the time-mean and the prime denotes the transient state.

Substituting Eq.(6.2) into Eq.(6.1) and taking the time average gives the momentum equation for stationary jet stream

$$\underset{A}{f (\bar{v} - \bar{v}_g)} + \underset{B}{\left(-\bar{u}\frac{\partial \bar{u}}{\partial x} - \bar{v}\frac{\partial \bar{u}}{\partial y} \right)} + \underset{C}{\left(-\frac{\partial \overline{u'^2}}{\partial x} - \frac{\partial \overline{u'v'}}{\partial y} \right)} = 0 \tag{6.3}$$

where term A is the Coriolis torque due to the ageostrophic wind, term B is the advection of mean momentum by the mean flow, and term C is the eddy momentum flux convergence. As proposed by Namias and Clapp (1949) and discussed by Wallace (1978), the transient eddy flux (term C) is likely to be an order of magnitude smaller than the other terms for a stationary jet stream. The governing equation for transients is easily obtained

by subtracting the mean-state Eq.(6.3) from Eq.(6.1). We obtain

$$\frac{du'}{dt} = fv_a' + \underbrace{\left(-u'\frac{\partial \bar{u}}{\partial x} - v'\frac{\partial \bar{u}}{\partial y} \right)}_{B1 \quad B2} + \underbrace{\left(\frac{\partial \overline{u'^2}}{\partial x} + \frac{\partial \overline{u'v'}}{\partial y} \right)}_{C} \qquad (6.4)$$

A

where $v_a'(= v' - v_g')$ is the transient ageostrophic meridional wind component, which can be approximated by the transient part of the divergent component of the meridional wind v_χ'. Term A represents the Coriolis torque and terms B1 and B2 are the advection of the momentum of mean flow by the transient eddies. Term C can be viewed as the conversion of momentum between the mean flow and the transient eddies. It has been demonstrated that the variance due to the low-frequency, especially 15-30 days variation is much larger than that due to high-frequency variation (Murakami, 1981; Pan and Zhou, 1985). Therefore, Eq.(6.4) is appropriate for examining the balance of forces governing the long-term variations of the jet stream.

In a Lagrangian view, the magnitude of acceleration of the air entering the entrance region of the jet streak depends upon the inhomogeneous terms at the right hand side of Eq.(6.4) while the trajectory of the air can be determined by the characteristics of

$$\frac{dy}{dx} = \frac{v(x,y,t)}{u(x,y,t)} \qquad (6.5)$$

where $\frac{dy}{dx}$ is the direction of total horizontal wind. The results in Fig. 5.1 and 5.4 suggest that the Coriolis forcing is important to accelerate the air entering the entrance region of jet streaks. The relationship between streamline and trajectory for a moving system can be given as (Holton, 1979)

$$R_s = R_t \left(1 - \frac{C \cos \gamma}{V} \right) \qquad (6.6)$$

where

R_s = curvature of streamline

R_t = curvature of trajectory

C = moving speed of the system

γ = angle between streamlines and the direction of motion of the system

Since the propagation speed of the jet streaks is quite slow, the curvature of the trajectory and that of streamline is little different. Thus, to approximately determine the trajectory of air entering the jet, we may look at a synoptic map of the total 200mb wind. For example, Fig. 6.1 and 6.2 show the total 200mb wind on MONEX day 45 and day 77, both of which have maximum amplitude for the v_χ' pattern shown in Fig. 5.4.a. Both maps show that the air originating from the region of 15–20°N, 100°E takes an anticyconically curved path as it enters the jet stream.

The advection of mean momentum by the transient eddies (term B1) may become substantial near the jet stream region when the amplitude of transient eddy becomes large. To understand this effect, consider the following equation:

$$\frac{du'}{dt} = -u' \frac{\partial \bar{u}}{\partial x} \qquad (6.7)$$

Assume $\frac{\partial \bar{u}}{\partial x}$ is nearly constant in the jet region, then Eq.(6.7) can be solved analytically using the method of characteristics (Guenther and Lee, 1988). The solution turns out to be

$$u'(x,y,t) = u'(x_o,y_o,t_o)\ \exp\left(-\frac{\partial \bar{u}}{\partial x}\ \Delta t \right) \qquad (6.8)$$

where

$\Delta t = t - t_o$

(x_o, y_o) = the initial location of the air

The solution is satisfied along the characteristics (trajectory) $\frac{dy}{dx} = \frac{v(x,y,t)}{u(x,y,t)}$.

Over the entrance region of the stationary jet stream, $\frac{\partial \bar{u}}{\partial x}$ is positive, therefore the transient westerly momentum on an air parcel would tend to decay with time due to term B1. Over the jet exit region, $\frac{\partial \bar{u}}{\partial x}$ is negative, hence the disturbance u' of an air parcel would tend to grow exponentially with time. Far away from the jet axis, $\frac{\partial \bar{u}}{\partial x}$ is quite small as shown in Fig. 4.1 and term B1 is of little importance.

To understand the effect of term B2, let us assume that $v' \cong v_a' \cong v_\chi'$. Then, when a pair of meridional divergent wind disturbances is situated in the jet streak entrance region with southerly v_χ' to the south of the jet axis and northerly $v_\chi'$to the north of the jet stream, the value of B2 tends to be negative

everywhere. This tends to reduce the intensity of the jet stream. Term B2 tends to be positive everywhere in the exit region of the jet streak.

A rough estimate of terms A, B1, and B2 can be made for the spatial pattern shown in Fig. 5.4.a, which is associated with a westerly jet streak near the center of the domain. In the entrance region of the jet streak near 15^{o}N, 100^{o}E, A and B2 are on the order of $6x10^{-5}$ and $-3x10^{-5}$ ms^{-2} respectively, while B1 is negligible. Therefore, the air in this region experiences westerly acceleration. Near the center of the domain where the jet streak is located, A, B1 and B2 have the order of $5x10^{-5}$, $-3.5x10^{-5}$ and $-2x10^{-5}$ ms^{-2} respectively. This implies the increase of westerly momentum due to Coriolis force (term A) near the center of jet streak is mostly balanced by the decrease due to the advection of mean momentum by transient eddies (terms B1 and B2).

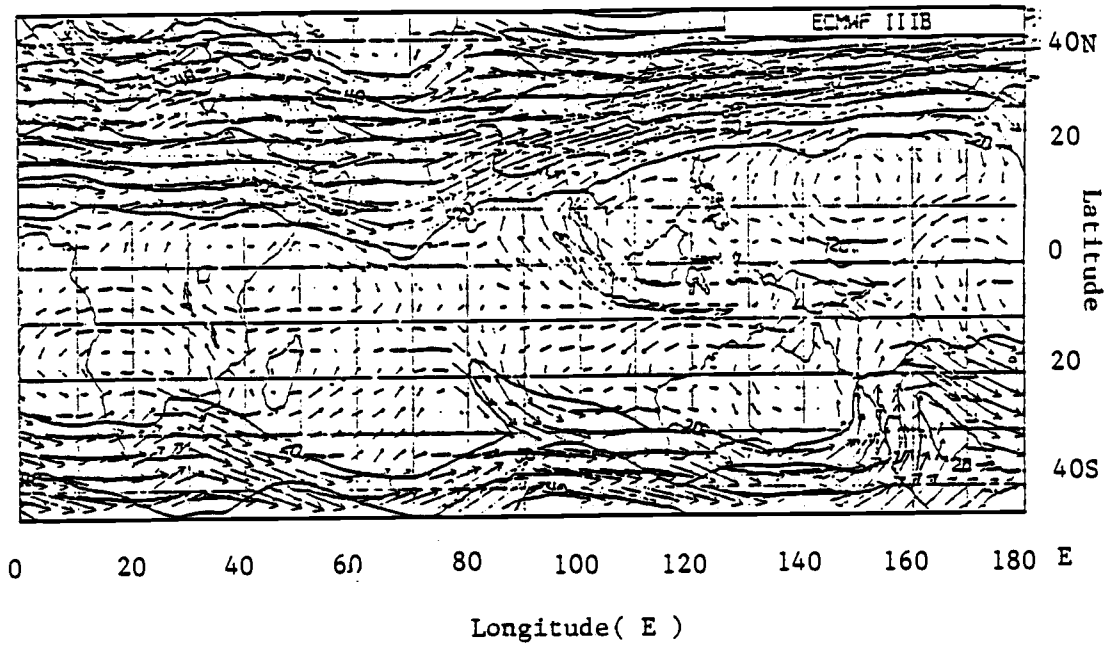

Fig.6.1 200mb wind from the FGGE IIIb data set on day 45, January 14, 1979.

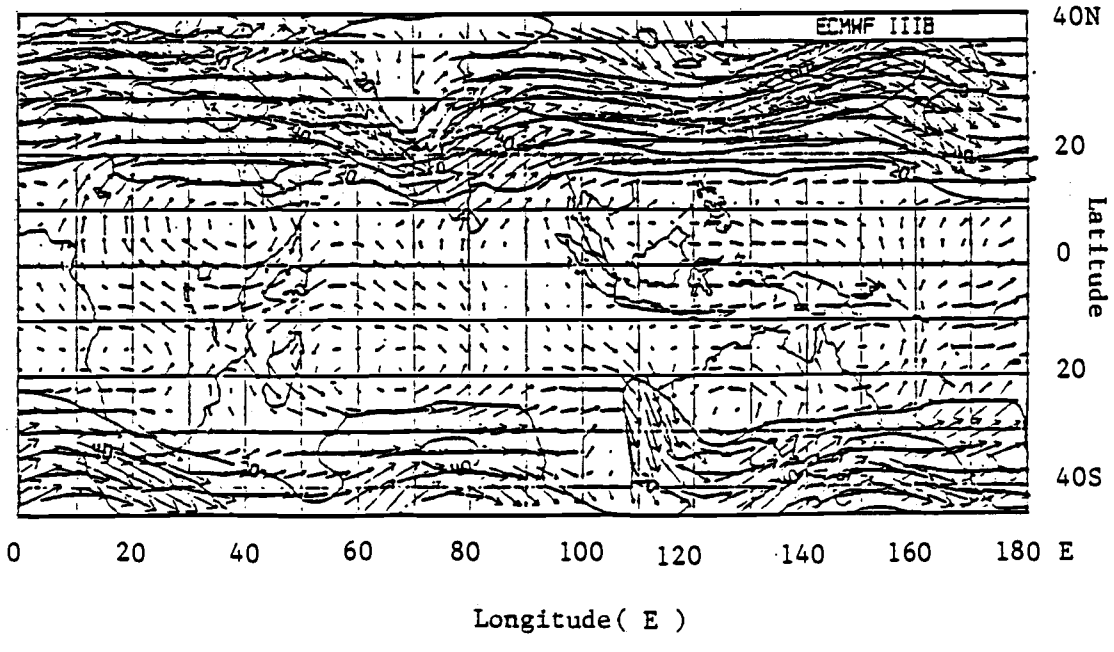

Fig.6.2 Same as Fig.6.1 except for on day 77, February 15,1979.

CHAPTER 7: SUMMARY

Taking advantage of the rotated principal component analysis, the 200mb low-pass filtered u_ψ' and v_χ' have been analyzed. The long-term variations of jet stream are found to be primarily due to the slowly eastward-moving jet streaks. The jet streak is associated with the pair-like disturbances of v_χ' and they propagate eastwards in a consistent way. The implied circulation transverse to the jet streak is thermally direct in the entrance region and thermally indirect in the exit region. The scale of the secondary circulation associated with the jet streak is about 20 degrees in the meridional direction. The pair-like eastward-propagating disturbances of $u_\psi'$and v_χ' that are isolated by the rotated principal component analysis can also be seen in the time-longitude and time-latitude cross-sections of u_ψ' and v_χ'.

The momentum equation governing the transient accelerations of air parcels in the jet streak shows that the magnitude of acceleration depends upon the Coriolis force due to the transient ageostrophic flow, the advection of mean momentum by the transient eddies, and the conversions of momentum between the mean flow and the eddies by means of eddy momentum flux convergence. The trajectory of the air experiencing these forcings is determined by the direction of total wind and depends upon the initial location where the air originates. In the entrance region of the jet streaks studied here, there is westerly acceleration due to

Coriolis force. Near the center of jet streak, the increase of westerly momentum due to Coriolis force is mostly balanced by the decrease due to the mean momentum advection by transient eddies.

REFERENCES

Bjorheim, K., P. Julian, M. Kanamitsu, P. Kallberg, P. Price, S. Tracton, and S. Uppala, 1981: FGGE III-B Daily Global Analysis. ECMWF.

Blackburn, M., 1985: Interpretation of ageostrophic winds and implication for jet stream maintenance. *J. Atmos. Sci., 42,* 2604-2620.

Blackmon, M. L., J. M. Wallace, N.-C. Lau, and S. L. Mullen, 1977: An observational study of the northern hemisphere wintertime circulation. *J. Atmos. Sci., 34,* 1040-1053.

Bourke, W., B. McAvaney, K. Puri, and R. Thurling, 1977: Global modeling of atmospheric flow by spectral methods. *Methods in Computational Physics, Vol. 17,* Academic Press, New York, 267-324.

Chang, C.-P., and K.-M. Lau, 1980: Northeasterly cold surges and near-equatorial disturbances over the winter MONEX area during December 1974. Part II: Planetary-scale aspect. *Mon. Wea. Rev., 108,* 298-312.

Guenther, R. B., and J. W. Lee, 1988: Partial Differential Equations of Mathematical Physics and Integral Equations. Prentice-Hall, New Jersey, 544pp.

Guillemin, E. A., 1957: Synthesis of Passive Networks. John Wiley and Sons, New York, 599-607.

Harman, H. H., 1960: Modern Factor Analysis. The University of Chicago Press, Chicago, 469pp.

Holton, J. R., 1979: An Introduction to Dynamic Meteorology. Academic Press, New York, 391pp.

Horel, J. D., 1981: A rotated principal analysis of the interannual variability of the northern hemisphere 500mb height field. *Mon. Wea. Rev., 109,* 2080-2092.

Lau, K.-M., C.-P. Chang, and P. H. Chan, 1983: Short-term planetary-scale interactions over the tropics and mid-latitudes. Part II: Winter-MONEX period. *Mon. Wea. Rev., 111,* 1372-1388.

Lau, N.-C, and K.-M. Lau, 1984: The structure and energetic of midlatitude disturbances accompanying cold air outbreaks over East Asia. *Mon. Wea. Rev., 112,* 1309-1327.

Murakami, T., 1981: Orographeric influence of the Tibetan Plateau on the Asiatic winter monsoon circulation. Part I: Large-scale aspects. *J. Meteor. Soc. Japan, 59,* 40-65.

Murakami, T., and A. Sumi, 1981: Large-scale aspects of the 1978-79 winter circulation over the Greater WMONEX region. Part II: Long-period perturbations. *J. Meteor. Soc. Japan, 59,* 646-671.

Namias, J. and P. F. Clapp, 1949: Confluence theory of high tropospheric jet streams. *J. Meteor., 6,* 330-361.

Pan, H.-L, F.-X. Zhou, 1985: The 10-20 day tropical-midlatitude interactions during the winter monsoon season. *J. Meteor. Soc. Japan, 63,* 829-844.

Pan, H.-L, 1987: Winter-time 10-20 day variations in the upper troposphere. *J. Meteor. Soc. Japan, 65,* 587-603.

Preisendorfer, R. W., F. W. Zwiers, and T. P. Barnett, 1981: Foundations of Principal Component Selection Rules. *SIO Reference series 81-4, Scripps. Insti. Ocn.*, University of California.

Richman, M. B., 1986: Rotation of principal components. *J. Climato., 6,* 293-335.

Shank, J. L., 1967: Recursion filters for digital processing. *Geophysics, 32,* 33-51.

The Numerical Algorithms Group, 1987: The NAG Fortran Library. The Numerical Algorithms Group Inc.

Wallace, J. M., 1978: A historical introduction .The general circulation-theory, modeling, and observations. NCAR.

APPENDIX

CROSS SPECTRAL ANALYSIS

The cross spectrum for two time series X_t and Y_t (t = 1,2,....,n) is computed by using the NAG Fortran Library (1987):

$$F_{XY}(\omega) = \frac{1}{2\pi n}\left[\sum_{t=1}^{n} Y_t \exp(i\omega t)\right]\left[\sum_{t=1}^{n} X_t \exp(-i\omega t)\right]$$

$$= CF(\omega) + i\, QF(\omega)$$

where

ω = the frequency

$CF(\omega)$ = the sample co-spectrum

$QF(\omega)$ = the quadrature spectrum

Then, the cross-amplitude spectrum $A(\omega)$ and phase spectrum $P(\omega)$ can be computed:

$$A(\omega) = [\, CF^2(\omega) + QF^2(\omega)\,]^{1/2}$$

$$P(\omega) = \tan^{-1}\left[\frac{QF(\omega)}{CF(\omega)}\right]$$